Ore Geology Reviews 74 (2016) 101–121

Contents lists available at ScienceDirect

Ore Geology Reviews

journal homepage: www.elsevier.com/locate/oregeorev

Upgrading iron-ore deposits by melt loss during granulite facies metamorphism

Laura J. Morrissey [a,*], Martin Hand [a], Kathleen Lane [a], David E. Kelsey [a], Rian A. Dutch [a,b]

[a] School of Physical Sciences, University of Adelaide, Adelaide, South Australia 5005, Australia
[b] Geological Survey of South, Australia, Department for State Development, Adelaide, S.A. 5000, Australia

ARTICLE INFO

Article history:
Received 29 April 2015
Received in revised form 7 November 2015
Accepted 9 November 2015
Available online 10 November 2015

Keywords:
THERMOCALC
Magnetite
Iron ore
Melt loss
Partial melting
Pseudosection

ABSTRACT

Forward modelling of Fe-rich phyllite is used to evaluate the effects of partial melting and melt loss on the concentration of iron in the residual rock package, leading to enrichment in Fe-oxide minerals (magnetite and hematite). The effect of melt loss during prograde metamorphism to peak conditions of ~850 °C was modelled using a series of calculated pressure–temperature (*P–T*) phase diagrams (pseudosections). The results show that metapelitic rocks with lower iron content are more fertile, produce more melt and therefore show a more significant increase (up to 35%) in the Fe-oxide content in the residual (melt depleted) rock package. Rocks with primary Fe-rich compositions are less fertile, lose less melt and therefore do not experience the same relative increase in the amount of Fe-oxides in the residuum. The results of the modelling have implications for the formation of economic-grade iron ore deposits in metamorphic terranes. Fe-rich compositions that represent primary ore horizons prior to metamorphism may not experience significant enrichment. However, those horizons with lower primary iron contents may be significantly upgraded as a result of melt loss, thereby improving the overall grade of the ore system. The application of the modelling to the highly metamorphosed Palaeoproterozoic Warramboo magnetite–hematite deposit in the southern Gawler Craton suggests that melt loss during granulite facies metamorphism led to upgrading of sub-economic units within the low-grade Price Metasediments to form the economically viable granulite facies Warramboo ore system. The results of this study suggest that high-temperature metamorphic terranes offer attractive exploration targets for magnetite-dominated iron ore deposits.

1. Introduction

Hematite ore has traditionally been considered to be of greater economic importance than magnetite ore, as high-grade hematite ore contains fewer impurities and therefore has lower processing costs (McKay et al., 2014). Australia is one of the largest global producers of iron ore, and the dominant ore exported by Australia is hematite ore (McKay et al., 2014). However, there has been a gradual decrease over time in the discovery of large hematite ore bodies, as well as a decline in the quality of hematite ore exported from large-scale producers such as Australia (McKay et al., 2014; Mudd, 2010). As a result, magnetite deposits are increasingly generating economic interest, as simpler procedures for concentrating the ore allow for the formation of a high quality beneficiation product that attracts high prices (IronRoad, 2014; McKay et al., 2014). Magnetite deposits hosted in granulite facies rocks are additionally of economic interest, as the coarse-grained nature of the rock allows for easier concentration of the iron ore (e.g. IronRoad, 2014).

In the southern Gawler Craton, the Warramboo deposit is an example of an economic-grade, granulite facies, magnetite-dominant iron ore deposit (Figs. 1, 2). Recent work has correlated the magnetite gneisses at Warramboo to the Price Metasediments, a sequence of magnetite and hematite-bearing phyllites in the southern Gawler Craton (Fig. 1; Lane et al., 2015). The stratigraphic links between the greenschist facies Price Metasediments and the granulite facies magnetite gneisses that comprise the Warramboo deposit provide an opportunity to model the effect of high-grade metamorphism and partial melting on the iron concentration of a primary magnetite and hematite-bearing sedimentary package.

An average pelite may produce up to 50–60 vol.% total melt at conditions attainable during orogenesis (Clemens, 2006; Clemens and Vielzeuf, 1987). As melts are mobile, and many granites contain appreciable volumes of crustal material, volume reduction in the source region associated with melt loss is a mechanism to concentrate elements such as iron in the residual rock package (e.g. Brown, 2013; Droop et al., 2003; Redler et al., 2013; Sawyer, 1994; Vielzeuf and Holloway, 1988; White and Powell, 2002; Yakymchuk and Brown, 2014). For a layered sequence that contains variable amounts of magnetite and hematite, up to and including ore-grade concentrations, the concentration of iron as a result of melt loss may be an important process in improving iron ore grades.

* Corresponding author.
E-mail address: laura.morrissey@adelaide.edu.au (L.J. Morrissey).

http://dx.doi.org/10.1016/j.oregeorev.2015.11.012
0169-1368/

In this paper we investigate the effect of melt loss on bulk rock iron content ($Fe_2O_{3(TOTAL)}$) and the proportion of magnetite and hematite using samples from the Price Metasediments. The computed metamorphic phase diagrams from the greenschist facies Price Metasediments are compared with those using compositions from the residual (melt depleted) granulite facies Warramboo deposit to show that melt loss from the Price Metasediments is a plausible mechanism to upgrade subeconomic Fe-bearing sequences. We also model the effect of varying oxidation state of the bulk rock and its impact on the proportion of magnetite to hematite.

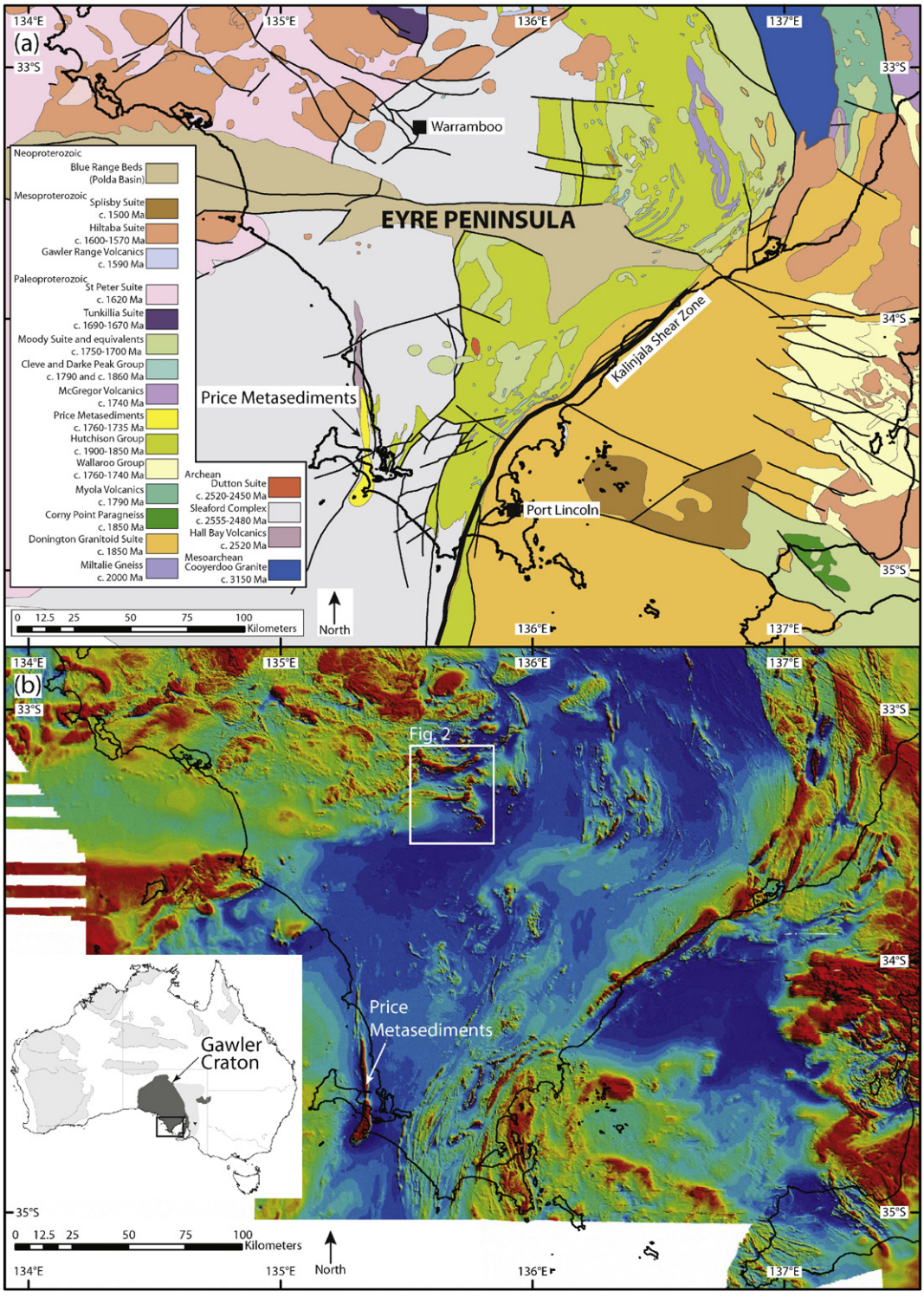

Fig. 1. Interpreted geology of the southern Gawler Craton, after Lane et al. (2015). b) TMI magnetic image of the southern Gawler Craton. (From SARIG <https://sarig.pir.sa.gov.au/Map>).

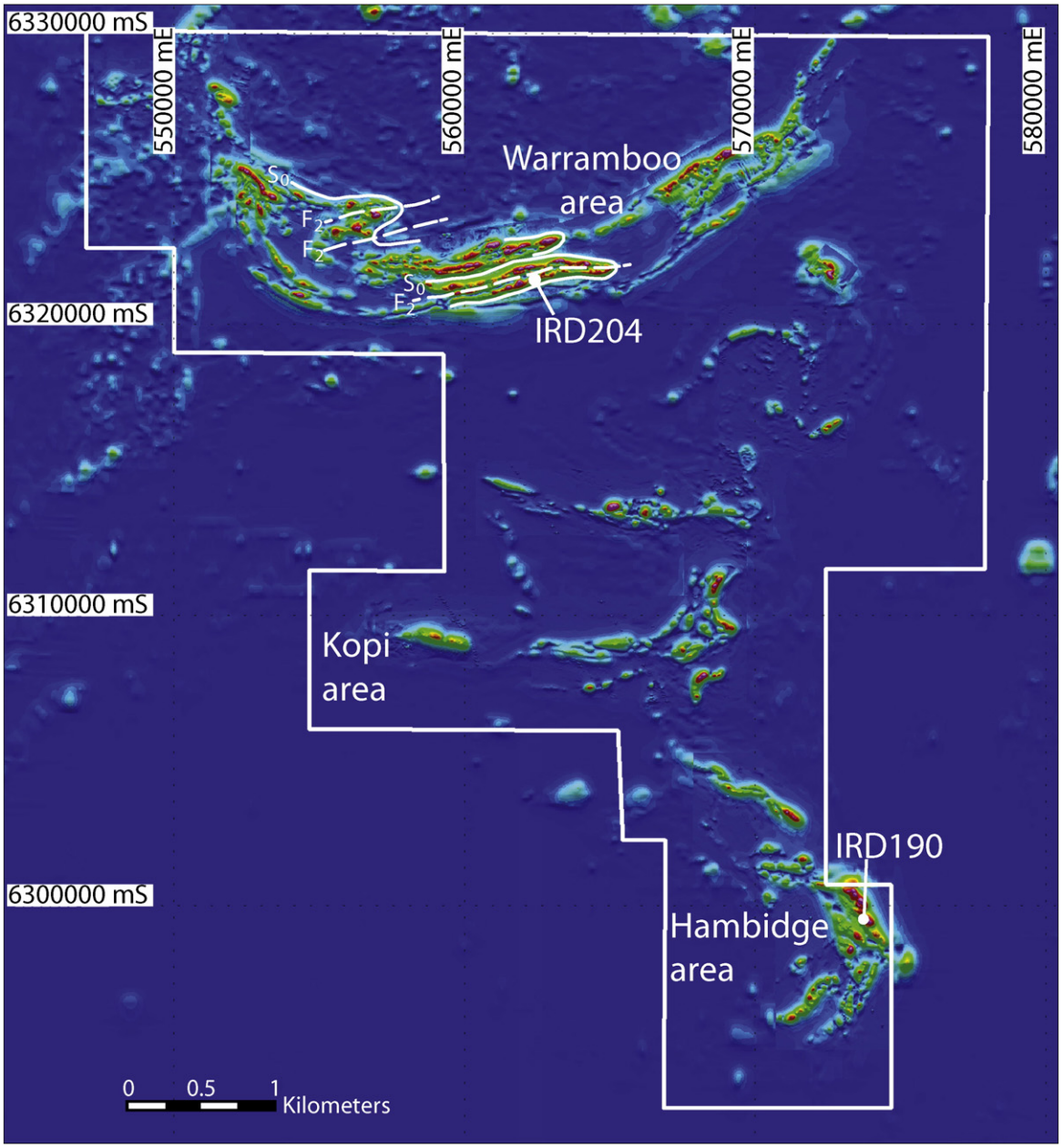

Fig. 2. Aeromagnetic image of Warramboo deposit, showing the Warramboo, Kopi and Hambidge deposits. Interpreted structural features of the Warramboo deposit are also shown, after Lane et al. (2015).

2. Geological setting

2.1. Gawler Craton

The Gawler Craton preserves a protracted geological history from c. 3150 Ma to c. 1450 Ma (Fig. 1; Daly et al., 1998; Fraser et al., 2010; Hand et al., 2007; Payne et al., 2009; Reid and Hand, 2012). The oldest rocks in the Gawler Craton are c. 3250–3150 Ma granitic gneisses that outcrop within a discrete shear-zone bounded tectonostratigraphic domain in the south-eastern Gawler Craton (Fraser et al., 2010). Seismic data suggests that these rocks may form the basement to a large part of the Gawler Craton (Fraser et al., 2010; Reid and Hand, 2012). The Neoarchean to earliest Paleoproterozoic Mulgathing Complex in the central-western Gawler Craton, and the Sleaford Complex in the southern Gawler Craton, dominantly comprise c. 2560–2480 Ma volcanic and sedimentary successions, as well as 2520–2420 Ma intrusive rocks, and are interpreted to represent portions of a single late Archean belt (Reid and Hand, 2012; Reid et al., 2014; Swain et al., 2005). Both these complexes were deformed and metamorphosed during the 2470–2410 Ma Sleafordian Orogeny (Daly et al., 1998; Dutch et al., 2010; McFarlane, 2006; Reid et al., 2014).

Following the Sleafordian Orogeny, the Gawler Craton experienced c. 400 Myr of tectonic quiescence. From c. 2000–1730 Ma, the tectonic setting of the western, northern and eastern Gawler Craton has been interpreted to have been dominantly extensional, with a series of rifting events resulting in basin development and widespread deposition of a number of volcanoclastic sedimentary sequences (Fig. 1; Fanning et al., 2007; Hand et al., 2007; Howard et al., 2011a; Howard et al., 2011b;

Payne et al., 2009; Reid and Hand, 2012). In central and western Eyre Peninsula, these include the c. 1760 Ma Price Metasediments (Fig. 1; Lane et al., 2015; Oliver and Fanning, 1997). In the northern Gawler Craton, magnetite-bearing metasediments with deposition ages of 1750–1730 Ma have been intersected in drill holes (Cutts et al., 2013; Payne et al., 2006; Payne et al., 2008); metasedimentary successions with depositional ages of 1760–1700 Ma are also found in the western Gawler Craton (Howard et al., 2011a).

Widespread basin development and sedimentation was terminated by the Kimban Orogeny at c. 1730–1690 Ma. The Kimban Orogeny was a craton-wide event that involved the development of crustal-scale shear zones, granitic magmatism and widespread metamorphism (e.g. Dutch et al., 2008; Dutch et al., 2010; Fanning et al., 2007; Hand et al., 2007; Howard et al., 2011b; Payne et al., 2008; Vassallo and Wilson, 2002). Preserved metamorphic conditions during the Kimban Orogeny vary widely, reflecting large exhumation gradients in the terrane (Dutch et al., 2008).

Following the Kimban Orogeny, the Gawler Craton was dominated by magmatic processes, with the formation of the c. 1690–1670 Ma Tunkillia Suite (Hand et al., 2007), the c. 1620 Ma St. Peter Suite (Swain et al., 2008) and at c. 1580 Ma the voluminous Gawler Range Volcanics and the Hiltaba Suite Granites (Daly et al., 1998; Fanning et al., 1988; Hand et al., 2007). Magmatism at c. 1580 Ma was accompanied by widespread, high-grade metamorphism in the northern and southeastern Gawler Craton (Cutts et al., 2011; Forbes et al., 2012; Morrissey et al., 2013; Payne et al., 2008).

2.2. Price Metasediment–Warramboo system

The Warramboo deposit consists of significant iron concentrations at Warramboo, Hambidge and Kopi in the central Eyre Peninsula (Figs. 1, 2). The deposits are entirely buried beneath Tertiary to Recent cover sequences, with mineralisation projected to occur at depths between 200 and 600 m (IronRoad, 2014). All samples used in this study come from exploration and resource-defining drilling. The iron deposits consist of granulite facies, magnetite-rich metapelitic gneisses interlayered with magnetite-poor felsic gneisses. The Warramboo deposit is the largest known magnetite deposit in Australia, with a resource of 3.7 billion tonnes at 16 wt.% Fe (IronRoad, 2014; Lane et al., 2015). The granulite facies host rock is coarse-grained and therefore the Fe-oxides are easier to concentrate. After concentration, it is estimated that the Warramboo deposit will produce a beneficiation product of 67% Fe (IronRoad, 2014).

The Warramboo deposit appears on regional aeromagnetic imagery as a series of east–west trending domains that outline an isoclinal fold system (Fig. 2; Lane et al., 2015). Although detailed geochronology and structural interpretation has focussed on the Warramboo area, the Hambidge area to the south preserves similar relationships and lithologies, and is therefore interpreted to correlate with the units in the Warramboo area.

The lithologies at Warramboo are described in more detail in Lane et al. (2015) and have been divided into magnetite-poor lithologies, magnetite-bearing horizons, and the magnetite-rich ore zones. The magnetite-poor lithologies include metasedimentary felsic gneiss, interpreted to have been deposited between 2470 and 2445 Ma, and two felsic, metaigneous units with magmatic ages of 2474–2466 Ma. The magnetite-poor lithologies were interpreted to be part of the Sleaford Complex of the southern Gawler Craton, and were deformed and metamorphosed at c. 2445 Ma during the Sleaford Orogeny (Lane et al., 2015). In contrast, the magnetite-bearing gneisses were interpreted to be a younger cover sequence, deposited between 1760 and 1735 Ma (Lane et al., 2015). The magnetite-bearing units are compositionally and mineralogically heterogeneous and contain horizons enriched in manganese that can be correlated across the deposit, interpreted to represent primary compositional layering inherited from a heterogeneous sedimentary package (Lane et al., 2015). Overall, the average grade of the magnetite gneisses of the Warramboo deposit is ~16 wt.% Fe (IronRoad, 2014).

The presence of detrital zircons within the Fe-rich units indicates they are clastic in origin. The detrital zircon age spectra are dominated by 1790–1750 Ma grains, similar to the greenschist facies, Fe-rich Price Metasediments in southern Eyre Peninsula (Fig. 1; Lane et al., 2015; Oliver and Fanning, 1997). In addition, the Price Metasediments and Warramboo magnetite-bearing gneisses have similar Sm–Nd isotopic compositions and both contain abundant spessartine-rich (i.e. Mn-rich) garnet, suggesting a common sedimentary source (Lane et al., 2015; Oliver and Fanning, 1997). Structurally, both the Price Metasediments and the Warramboo magnetite-gneisses are isoclinally folded and bounded by gneisses of the Sleaford Complex (Dutch et al., 2008; Lane et al., 2015). Therefore, the Warramboo gneisses are interpreted to be a high-grade correlative of the Price Metasediments.

Metamorphic zircon from the Warramboo deposit suggests it was deformed and metamorphosed at c. 1735 Ma during the Kimban Orogeny (Lane et al., 2015). However, there are no quantitative constraints on the pressure–temperature (*P–T*) conditions of the Warramboo deposit. Similarly, regional structural relationships indicate that the Price Metasediments were also deformed and metamorphosed during the Kimban Orogeny (Dutch et al., 2010). However, in contrast to the Warramboo deposit, the Price Metasediments are sub-to un-economic for iron ore. The purpose of this paper is to examine the impact of Kimban Orogeny metamorphism on the iron contents of the Price Metasediments, and the implications for concentrations of magnetite and hematite. This paper also provides the first quantitative constraints on the *P–T* conditions of the Warramboo deposit.

3. Sample descriptions

3.1. Price Metasediments

The Price Metasediments are characterised by fine-grained, grey-green, magnetite-bearing phyllite with a well-developed spaced cleavage (Oliver and Fanning, 1997). They are finely bedded and compositionally layered on a 1–10 mm scale. These compositional layers include aluminous pelite, psammite and layers that are very rich in Fe-oxide minerals. The Price Metasediments occur on aeromagnetic images as a prominent, north–south trending magnetic high in the southern Eyre Peninsula (Fig. 1). The chosen samples have been selected as representatives of comparatively magnetite-poor (sample 377514) and magnetite-rich layers (sample 377516) within the package. The abundances of magnetite and hematite were determined using point counting; abundances of the remaining minerals were determined using visual estimates.

3.1.1. Sample RS 377514 (53H 525844E 6159150S): magnetite-poor

Sample 377514 is fine-grained with mineralogical layering defined by muscovite-rich and quartz-rich layers (Fig. 3a). Muscovite is abundant (~50 vol.% of the sample), and occurs as small flakes (commonly <10 μm) that define a weak foliation in some layers. Quartz is also abundant (~30 vol.% of the sample) and occurs as anhedral grains ~50 μm size. Magnetite comprises 6–8 vol.% of the sample and occurs as small euhedral crystals, ranging in size from 10 to 200 μm, distributed throughout the thin section. Small, ragged grains of hematite are much less common than magnetite (<0.5 vol.% of the sample). Garnet occurs throughout the rock as equant euhedral crystals ~10–50 μm in size and may contain fine-grained inclusions of magnetite. Biotite occurs in minor amounts as small flakes up to 100 μm in size that are commonly unoriented. Chlorite occurs as flakes that are aligned with the foliation, or adjacent to garnet and magnetite and along biotite cleavage planes. Plagioclase occurs in both the muscovite- and quartz-rich domains.

3.1.2. Sample RS 377516 (53H 529725E 6159716S): magnetite-rich

Sample 377516 is compositionally layered, with layers 1–10 mm in width (Fig. 3b). The sample is dominantly comprised of inter-bedded pelitic and Fe-oxide-rich layers. The compositional layering is discordant to a weak foliation that is present in some layers. The pelitic layers

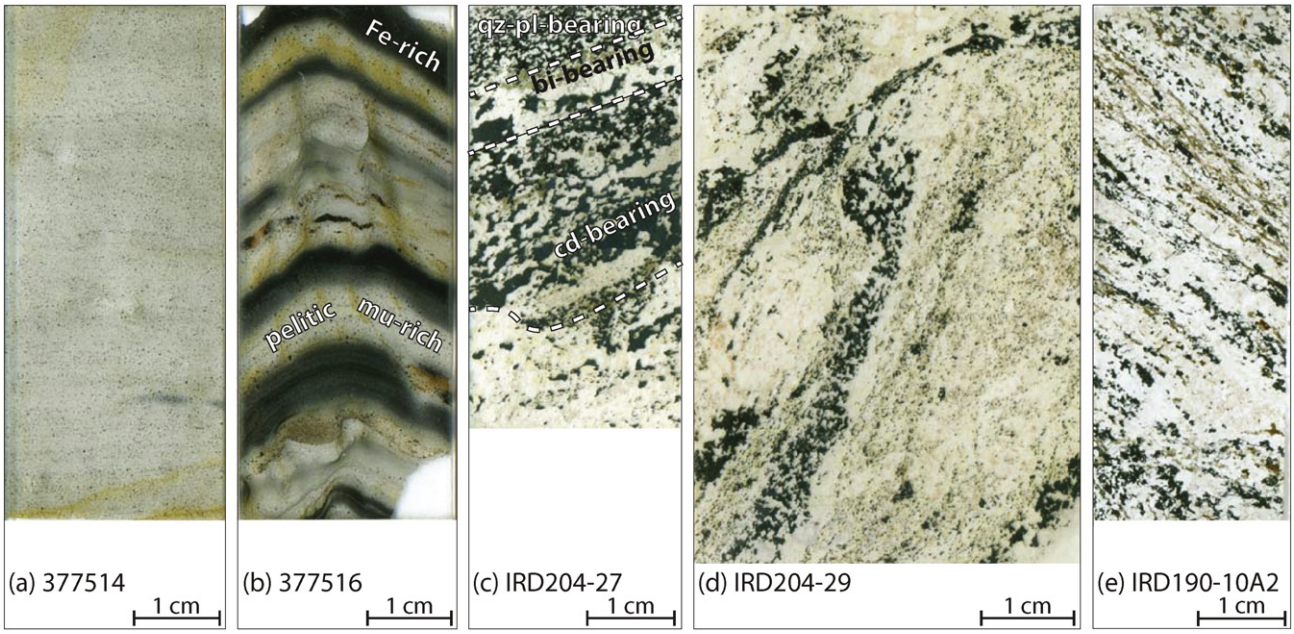

Fig. 3. Thin section images. a) sample 377514; b) sample 377516; c) sample IRD204-27; d) sample IRD204-29; e) sample IRD190-10A2.

have similar mineralogy to sample 377514 and are dominated by quartz and muscovite, with euhedral magnetite (100–200 μm) and less common hematite distributed throughout the layers. Biotite flakes (up to 100 μm), and subordinate chlorite, occur in contact with magnetite porphyroblasts. Small euhedral garnet grains (up to 100 μm) occur throughout the sample, but are more common in the pelitic horizons. The Fe-oxide-rich layers contain abundant magnetite and hematite (up to ~40 vol.% of the layer), small anhedral quartz grains and biotite flakes that occur in contact with magnetite. Magnetite is the dominant oxide in these layers and occurs as porphyroblasts (100–200 μm), whereas hematite occurs as smaller, elongate grains. The sample also contains an apatite-rich layer, as well as layers dominantly comprised of quartz and plagioclase. These layers also contain magnetite and small biotite flakes (50 μm) that define a weak foliation. Although the sample has lithological, and hence mineralogical, domains, on a thin section scale it contains ~15–16 vol.% Fe-oxides (approximately 70% magnetite to 30% hematite).

3.2. Warramboo gneisses

The magnetite-bearing units from the Warramboo deposit range from sparsely magnetite-bearing to magnetite-rich ore, but at the metre-scale all lithologies contain deformed K-feldspar–quartz ± plagioclase leucosomes and variable abundances of hematite and spessartine-rich garnets (Lane et al., 2015). Two samples from the Warramboo area (samples IRD204-27 and IRD204-29) and one sample from the Hambidge area (sample IRD190-10A2) were selected for modelling. The magnetite-bearing gneisses in the Hambidge area contain similar mineral assemblages to the gneisses from the Warramboo area but are variably retrogressed, with alteration of cordierite to pinite and replacement of feldspars in some samples. The abundances of magnetite and hematite were determined using point counting.

3.2.1. Sample IRD204-27 (53H 562340E, 6321437S)

Sample IRD204-27 was collected from exploration drill hole IRD204, depth interval 237.8–237.9 m. The sample contains interlayered Fe-oxide-rich pelitic and psammitic horizons and Fe-oxide poor quartzofeldspathic leucosomes on a scale from a few millimetres to 2 cm in thickness. The sample is very rich in magnetite and hematite, which together comprise ~30 vol.% of the sample (Fig. 3c).

In the Fe-oxide-rich psammitic horizons, hematite and magnetite grains (<1 mm in diameter) occur in approximately equal proportions, together with abundant quartz, plagioclase, minor euhedral garnet (<100 μm) and rare apatite (Fig. 4a–b). Magnetite may be separated from quartz by thin coronae of plagioclase (Fig. 4a–b). The Fe-oxide-rich pelitic horizons are predominantly composed of cordierite, magnetite and hematite. Hematite is the dominant Fe-oxide and forms coarse grains up to 5 mm (Fig. 4a). Cordierite occurs as coarse-grained (up to 5 mm) porphyroblasts that contain inclusions of magnetite, elongate, euhedral hematite, patches of sillimanite and quartz. Fine-grained cordierite also occurs as inclusions in hematite. Small euhedral garnet grains occur throughout the pelitic layers in contact with magnetite and hematite. The sample contains biotite (<7 vol.% of the sample), that occurs at the interface between the pelitic and psammitic horizons as coarse-grained flakes up to 2 mm (Fig. 3c) and as anhedral grains associated with magnetite and hematite in the pelitic layers. The Fe-oxide-poor quartzofeldspathic leucosomes in this sample are ~3 mm in width and dominantly composed of K-feldspar and quartz with minor cordierite and rare plagioclase.

3.2.2. Sample IRD204-29 (53H 562340E, 6321437S)

Sample IRD204-29 was collected from exploration drill hole IRD204, depth interval 284.9–285 m and contains magnetite, hematite, cordierite, garnet, K-feldspar, plagioclase, minor biotite and sillimanite (Fig. 3d). Magnetite and hematite occur in approximately equal proportions and together comprise 15–18 vol.% of the sample. Coarse-grained magnetite and hematite are commonly intergrown with quartz and sometimes finer-grained plagioclase (up to 500 μm), and may be enveloped by cordierite. Garnet is abundant and occurs throughout the sample as euhedral grains ~250 μm in diameter and also as coronae on coarse-grained magnetite and hematite. Cordierite is abundant and occurs as porphyroblasts (up to 1 cm) that include small, foliation-parallel hematite grains, patches of foliation-parallel sillimanite and horizons of euhedral garnet (Fig. 4c–d). The sample contains quartzofeldspathic leucosomes that are composed of coarse-grained microcline and perthitic K-feldspar (up to 3.5 mm in diameter), quartz (up to 1.5 mm) and variable amounts of plagioclase. Sillimanite is abundant and occurs as patches in cordierite (Fig. 4c–d) or as aligned aggregates with hematite and magnetite (up to 3 mm in length; Fig. 4e–f). Less commonly, it occurs as

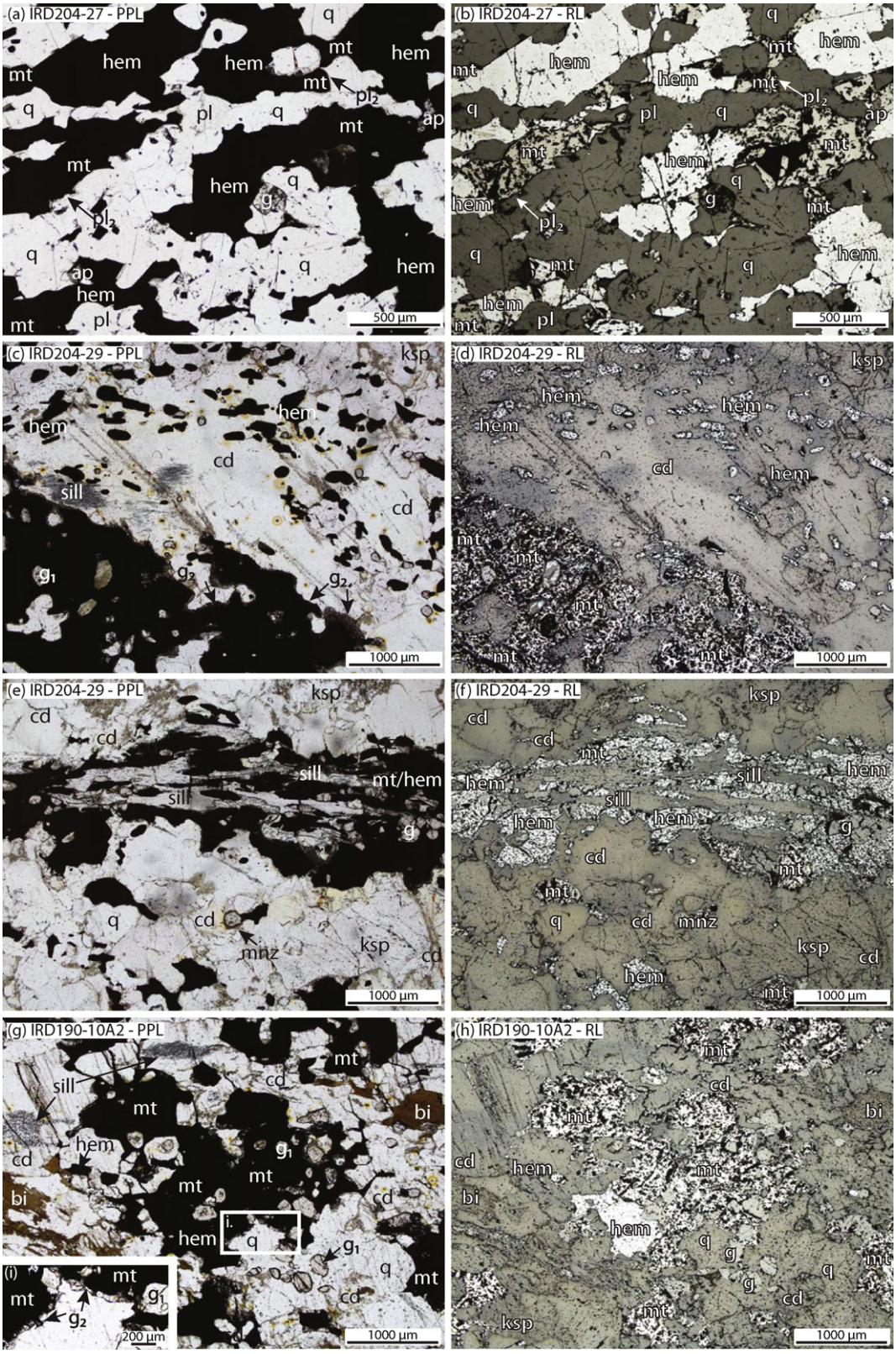

Fig. 4. Photomicrographs showing representative mineral relationships. Each photomicrograph is shown in plain polarised light and reflected light. a–b) sample IRD204-27: Fe-oxide-rich psamitic horizon, dominantly comprised of quartz, magnetite, hematite and minor plagioclase and garnet. Plagioclase coronas (pl_2) separate magnetite and quartz. c–d) sample IRD204-29: fine-grained patches of sillimanite are included in cordierite and are common near magnetite/hematite. Euhedral garnet and cordierite are included in magnetite/hematite, and a second generation of garnet forms coronas on magnetite/hematite porphyroblasts. e–f) sample IRD204-29: sillimanite associated with magnetite/hematite aggregates aligned with the gneissic foliation, euhedral garnet is also included in magnetite/hematite. Cordierite is abundant and partially envelops magnetite/hematite. g–h) sample IRD190-10A2: euhedral garnet inclusions in magnetite/hematite. A second generation of garnet occurs as coronas on magnetite/hematite. Cordierite includes patches of aligned sillimanite and partially envelops magnetite/hematite. i) Inset image in the bottom left corner of Fig. 4g, showing the secondary garnet coronas in more detail.

inclusions in quartz or K-feldspar or along grain boundaries of cordierite and quartz.

3.2.3. Sample IRD190-10A2 (53H 573640E, 6299430S)

Sample IRD190-10A2 was collected from exploration drill hole IRD190, depth interval 237.6–241.76 m. This sample contains a gneissic foliation defined by magnetite–hematite-rich layers and quartzofeldspathic leucosomes (Fig. 3e). Small, euhedral garnet grains (250 μm, rarely up to 500 μm) occur in discrete layers commonly associated with magnetite and hematite (Fig. 4g–h). They may occur included in magnetite and hematite, cordierite and K-feldspar. Cordierite is abundant and contains patches of fine-grained sillimanite, which are commonly parallel to the gneissic fabric. The patches of fine-grained sillimanite included in cordierite are more abundant in the magnetite and hematite-rich layers, and in these layers cordierite commonly envelops magnetite and hematite. Cordierite also occurs within the quartzofeldspathic leucosomes, together with abundant perthite (up to 3 mm in diameter), quartz (up to 2 mm) and less common antiperthite and plagioclase (up to 750 μm). Magnetite and hematite are abundant (~13 vol.%, with magnetite the dominant oxide) and occur as euhedral grains that are parallel to the foliation (300–800 μm) and coarse anhedral porphyroblasts (up to 3 mm). Coarse-grained magnetite and hematite contain inclusions of garnet, quartz (~100 μm) and rare euhedral biotite and cordierite. A second generation of garnet occurs as thin (<50 μm) coronae on magnetite and hematite grains (shown in the inset image in Fig. 4g) and in places magnetite and hematite are separated from coarse-grained euhedral garnet by a corona of cordierite and garnet (Fig. 4g–h). Biotite forms anhedral flakes commonly associated with magnetite, hematite and garnet. It also occurs in domains as elongate grains (up to 1.5 mm in length and 250 μm in width), associated with elongate magnetite and hematite (Fig. 3e).

4. Metamorphic modelling

Although it cannot be definitively proven that the magnetite-rich gneisses that form the Warramboo deposit and the sub-economic Price Metasediments are the same Fe-rich sequence, the similarity in depositional age, detrital zircon populations, enclosing basement and Nd isotopic composition between the two argues that they are part of the same sequence (Lane et al., 2015). The Warramboo gneisses contain quartzo-feldspathic leucosomes, suggesting they have melted. They also preserve granulite facies mineral assemblages typical of aluminous metasedimentary rocks (i.e. garnet–cordierite–sillimanite-bearing; White et al., 2001) with little (<10 vol.%) biotite, and in general have compositions that are depleted in elements such as K_2O when compared to the Price Metasediments (Table 1; Oliver and Fanning, 1997). These features are consistent with melt loss from a sedimentary protolith during high-temperature metamorphism (e.g. Diener et al., 2008; Powell and Downes, 1990; White and Powell, 2002). The purpose of this study is to use the sub-economic Price Metasediments and their economic granulite facies equivalents as a case study to investigate the general process of Fe-oxide enrichment as a result of melt loss during high-grade metamorphism.

For the purposes of the phase equilibria modelling, mol% and vol.% are approximately equivalent. The following abbreviations are used: g = garnet; pl = plagioclase; liq = silicate melt; ep = epidote; ksp = K-feldspar; bi = biotite; opx = orthopyroxene; cd = cordierite; mu = muscovite; chl = chlorite; mt = magnetite; ilm = ilmenite; hem = hematite; pa = paragonite; ab = albite; sill = sillimanite; and = andalusite; ky = kyanite; q = quartz.

4.1. Determining the conditions of metamorphism of the Price Metasediments–Warramboo system

Pressure–temperature pseudosections were calculated for samples 377514 and 377516 (Price Metasediments) and IRD204-27, IRD204-29 and IRD190-10A2 (Warramboo gneisses). *P–T* pseudosections for the samples were calculated using THERMOCALC v3.40, using the internally consistent dataset, ds62, of Holland and Powell (2011) and the activity–composition (*a–x*) models re-parameterised for metapelitic rocks in the MnNCKFMASHTO system (Powell et al., 2014; White et al., 2014a; White et al., 2014b), where 'O' is a proxy for Fe_2O_3. Whole-rock chemical compositions for the calculation of metamorphic phase equilibria were determined by crushing up a representative amount of each sample (100–200 g) and using a tungsten carbide mill. Bulk-rock chemical compositions were conducted by Franklin and Marshall College, Pennsylvania. Major elements were analysed by fusing a 0.4 g portion of the powdered sample with lithium tetraborate for analysis by XRF. Trace elements were analysed by mixing 7 g of crushed rock power with Copolywax powder and measurement by XRF. The whole rock chemistry for each sample used in the calculation of the mineral equilibria pseudosections is given in Appendix 1.

The amount of H_2O and Fe_2O_3 in the bulk chemical composition that relates to the formation of the peak (i.e. maximum temperature) metamorphic mineral assemblages can be difficult to determine, due to hydration and oxidation during low-*T* processes such as weathering (e.g. Johnson and White, 2011). The proportion of Fe_2O_3 to FeO for all samples was evaluated using *T*–M_O sections (see below) and was determined based on the proportion of magnetite to hematite. Subsolidus metamorphism is interpreted to involve aqueous fluid-present mineral

Table 1
Bulk rock compositions in weight% for pseudosection modelling.

	773514: Price Metasediments				773516: Price Metasediments				IRD: Warramboo mt gneisses		
wt.%	Protolith	ML1	ML2	ML3	Protolith	ML1	ML2	ML3	204-27	204-29	190-10A2
SiO_2	58.51	58.04	56.33	54.87	57.74	57.32	56.69	55.98	41.97	50.27	53.11
TiO_2	0.55	0.57	0.67	0.74	0.46	0.48	0.50	0.54	0.77	0.93	0.42
Al_2O_3	15.58	15.72	16.07	16.24	11.00	10.93	10.76	10.57	7.83	13.56	12.24
Fe_2O_3	7.75	8.16	9.49	10.50	14.55	15.19	16.09	16.91	39.70	19.91	15.50
FeO	6.05	6.36	7.42	8.18	7.13	7.43	7.86	8.27	4.20	6.29	8.63
MnO	0.81	0.86	1.00	1.11	0.83	0.86	0.91	0.96	0.38	2.08	1.04
MgO	2.30	2.42	2.82	3.11	1.61	1.68	1.78	1.87	2.82	2.89	2.30
CaO	0.68	0.69	0.70	0.67	1.25	1.29	1.34	1.38	0.56	0.75	1.07
Na_2O	0.84	0.69	0.41	0.32	1.47	1.38	1.26	1.18	0.33	0.78	1.13
K_2O	4.62	4.62	4.34	3.99	2.68	2.57	2.39	2.20	0.94	2.19	3.85
H_2O	2.31	1.87	0.76	0.30	1.28	0.88	0.41	0.14	0.50	0.35	0.70
$Fe_2O_{3(TOTAL)}$	14.48	15.23	17.74	19.59	22.47	23.45	24.83	26.10	44.36	26.90	25.09
Melt lost (mol%)	–	6.40	17.40	11.30	–	5.50	7.20	6.20	–	–	–

assemblages, therefore the modelling of the Price Metasediments was done with water set in excess (i.e. always present across the subsolidus part of *P*–*T* space). Determining the appropriate amount of H_2O at peak conditions for granulite facies rocks is more problematic, as low-*T* retrogression and the presence of other volatiles such as CO_2, F and Cl means that the measured LOI may be an overestimation. Therefore, the H_2O

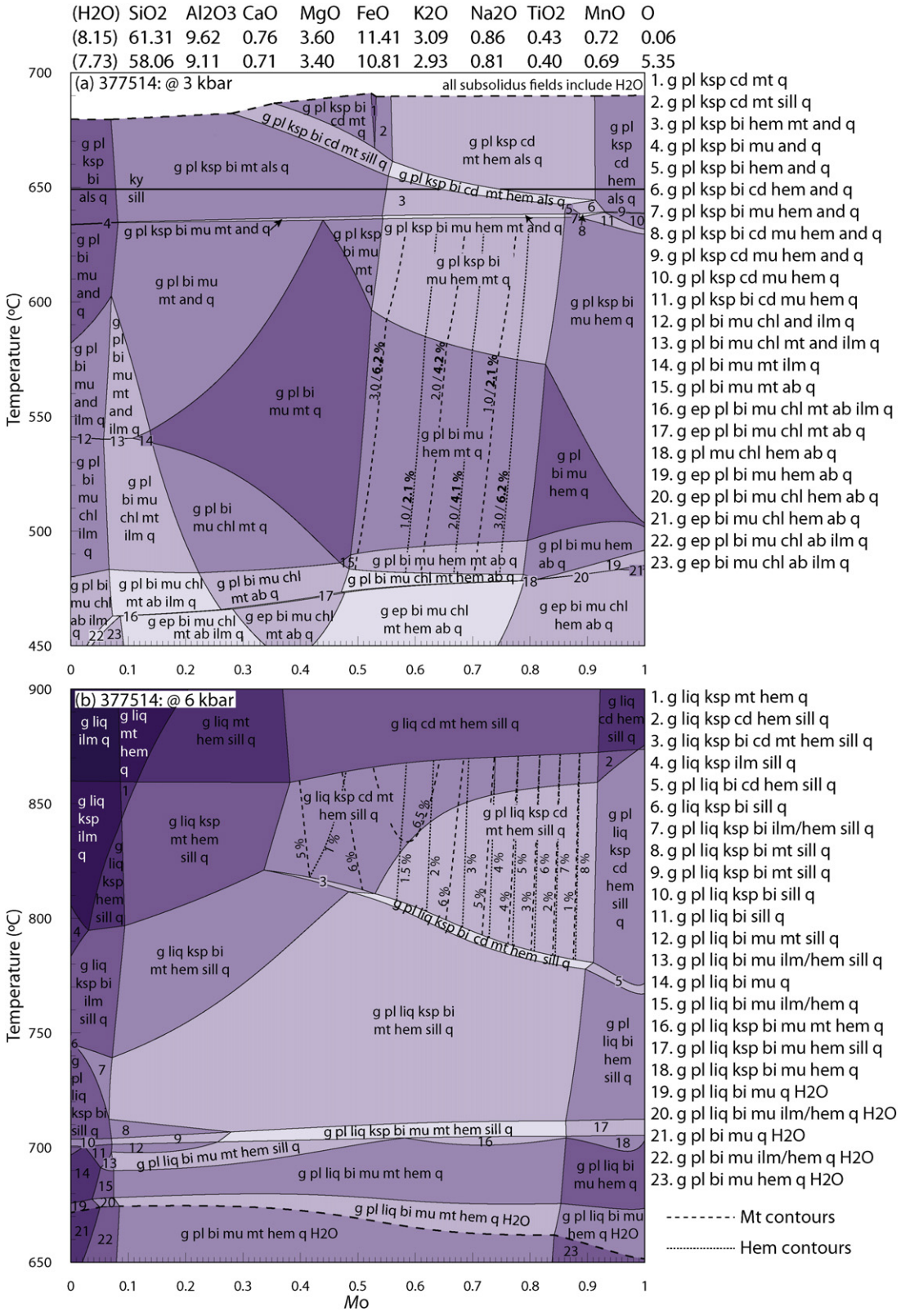

Fig. 5. *T*–M_O sections for samples 377514 and 377516. The compositions are given above each pseudosection. At $x = 0$, 1% of total Fe is modelled to be Fe^{3+}, whereas at $x = 1$, 99% of total Fe is modelled to be Fe^{3+}. The sections have been contoured for the proportion of magnetite to hematite. For the subsolidus sections with H_2O in excess, the amounts of magnetite and hematite are given including free water (regular text) and the absolute proportion not including free water (bold text). a) Sample 377514, at 3 kbar, with H_2O in excess. b) Sample 377514, at 6 kbar. c) Sample 377516, at 3 kbar, with H_2O in excess. d) Sample 377516, at 6 kbar.

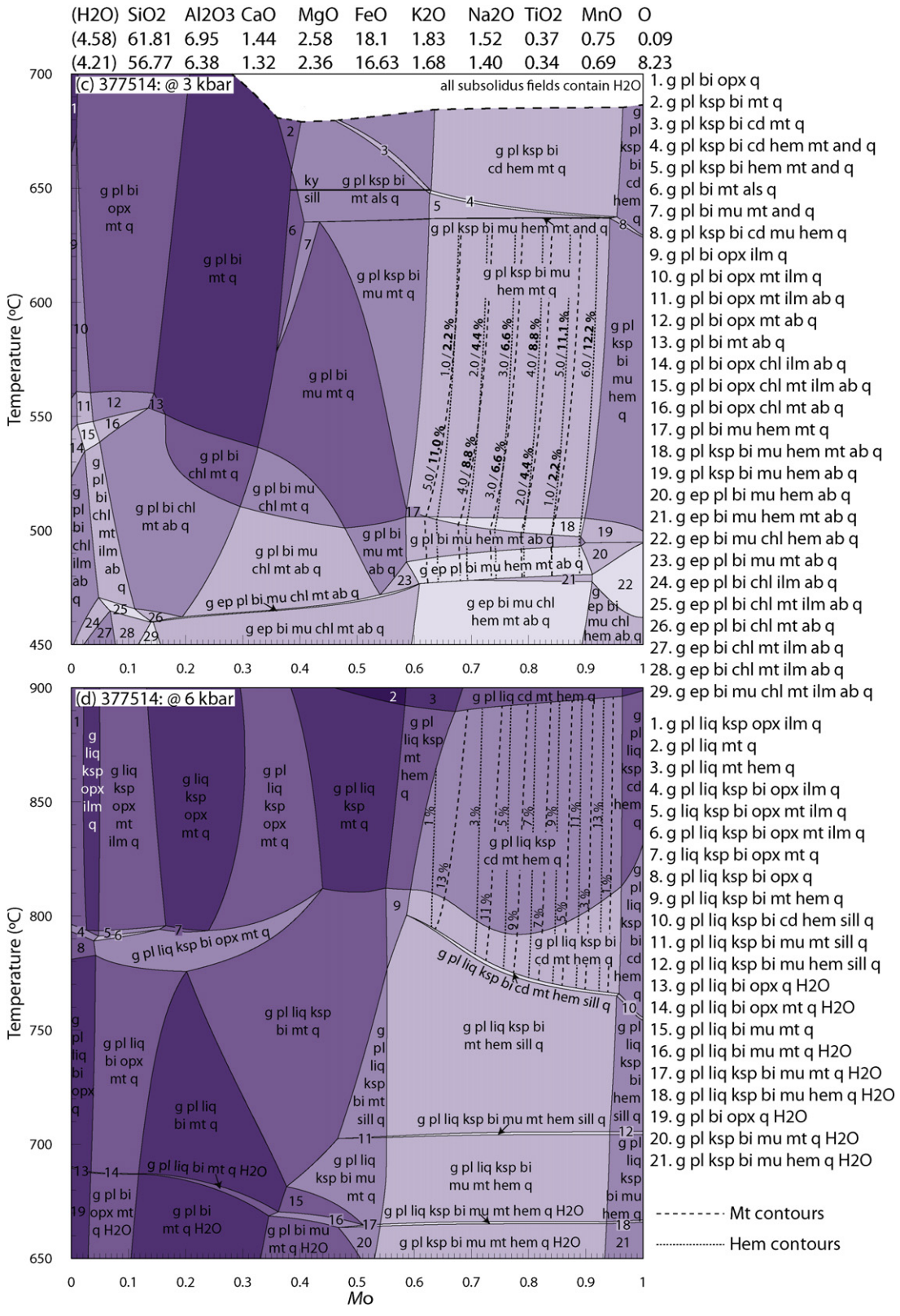

Fig. 5 (*continued*).

content of the Warramboo gneisses during peak metamorphism was estimated based on the modal proportion of H_2O-bearing minerals (biotite and cordierite) and a conservative estimate of the H_2O content of these minerals (Deer et al., 1992; Rigby and Droop, 2011).

4.2. Modelling the effects of melt loss

The amount and composition of melt within a given rock is dependent on the *P–T* conditions and the initial bulk rock composition of the

protolith, and may be modelled using a closed system (e.g. Johnson et al., 2008; Korhonen et al., 2010; White and Powell, 2002; Yakymchuk and Brown, 2014). However, the continental crust is an open system with respect to melt, whereby melt accumulates until it reaches a critical threshold and is then lost episodically from the source rock (Brown, 2010, 2013; Handy et al., 2001; Sawyer, 1994; Yakymchuk and Brown, 2014; Yakymchuk et al., 2013). A rock may experience a series of melt loss events throughout a single orogenic cycle, each of which modify the chemical composition and therefore fertility of the source rock (Brown, 2013; Korhonen et al., 2010; Vielzeuf et al., 1990; White et al., 2002; Yakymchuk and Brown, 2014). We investigate the effect of these melt loss events on the composition of the Price Metasediments using a series of *P–T* pseudosections and the interpreted peak conditions of the Warramboo deposit (as determined below). The amount of H_2O in the starting bulk composition is based on LOI, the amount of starting Fe_2O_3 was determined based on the proportion of magnetite to hematite (as above).

5. Results of metamorphic modelling

5.1. The effect of oxidation state

Before determining the likely *P–T* conditions of the Price Metasediments and the Warramboo deposit, it is necessary to explore the effect of variable oxidation state of the bulk rock composition on the mineralogy. The oxidation state of the rock composition can have a significant effect on the stability of mineral assemblages (e.g. Boger et al., 2012; Diener and Powell, 2010; Johnson and White, 2011; Johnson et al., 2008; Lo Pò and Braga, 2014; Morrissey et al., 2015). This is because highly oxidised rocks contain elevated levels of Fe_2O_3, which favours the stability of minerals like magnetite and hematite that sequester Fe, resulting in the growth of comparatively Mg–Al enriched minerals such as cordierite in the silicate-dominated part of the assemblage. Determination of Fe_2O_3 by titration may overestimate the amount of Fe_2O_3 in the bulk rock due to low-*T* oxidation during weathering, or oxidation during sample preparation for geochemical analysis (e.g. Johnson and White, 2011; Lo Pò and Braga, 2014). Therefore, the effect of varying the Fe_2O_3 amount was investigated using *T*–M_O sections for both samples of the Price Metasediments (samples 377514 and 377516), where $x = 0$ is equivalent to 1% of total iron being Fe_2O_3 and 99% being FeO; and $x = 1$ equivalent to 99% of total iron being Fe_2O_3 and 1% being FeO (Fig. 5). The *T*–M_O sections were calculated at pressures of 3 kbar to investigate the effect of oxidation state on the original greenschist facies assemblages, and at 6 kbar using the original protolith compositions above the solidus prior to melt loss.

For sample 377514, the magnetite–hematite-bearing fields occur between $M_O = 0.49$–0.80; similarly sample 377516 requires $M_O = 0.59$–0.90 (Fig. 5a, c). Varying the oxidation state within this interval does not significantly affect the total amount of these oxides, but does affect the proportion of magnetite to hematite. In highly oxidised compositions hematite is the dominant oxide, whereas magnetite is more abundant in less oxidised compositions. Within the magnetite–hematite field, varying the amount of Fe_2O_3 slightly affects the pressures and temperatures of the main silicate boundaries, but does not affect the stable phase assemblages.

5.2. Metamorphic conditions of the Price Metasediments

It is necessary to determine the pressure–temperature (*P–T*) evolution and conditions of metamorphism of the Price Metasediments and the Warramboo deposit to provide a framework for modelling the effects of melt loss.

5.2.1. Sample 377514

The peak metamorphic assemblage is interpreted as garnet, quartz, muscovite, hematite, magnetite, plagioclase, chlorite and minor biotite. This assemblage occurs in a narrow triangular field from ~450–470 °C and pressures less than 4 kbar (Fig. 6a). This assemblage is predicted to contain 5.2 mol% magnetite and 1.6 mol% hematite, excluding excess H_2O as a free fluid phase. With increasing temperature, the total amount of Fe-oxide minerals remains approximately constant at ~6.7 mol%, but the proportion of magnetite to hematite increases with temperature (Fig. 7a). The total amount of Fe-oxides modelled (~6.8 mol%) is consistent with observations (~6–8 vol.%; Fig. 3a).

5.2.2. Sample 377516

The peak metamorphic assemblage is interpreted as garnet, muscovite, magnetite, hematite, quartz, plagioclase and minor biotite. The absence of epidote and K-feldspar suggest that the mineral assemblage formed at 465–535 °C and 2–5 kbar (a narrow, triangular field in Fig. 6b, consistent with the conditions inferred for sample 377514). The mineral assemblage in this field is predicted to contain ~9.2–9.4 mol% magnetite and ~3.3 mol% hematite, excluding excess H_2O as a free fluid phase. The total amount of Fe-oxides modelled (12.5–13 mol%) is broadly consistent with that observed (15–16 vol.%; Fig. 3b).

5.3. Metamorphic conditions of Warramboo deposit

5.3.1. Sample IRD204-27

The peak metamorphic assemblage is interpreted as garnet, plagioclase, K-feldspar, cordierite, magnetite, hematite, quartz and silicate melt. The presence of cordierite and absence of sillimanite constrains pressures to below 7.8 kbar (Fig. 7a). In this sample, the biotite-out boundary occurs at 840–850 °C. Biotite in this sample is typically anhedral and intergrown with magnetite–hematite or occurs at the interface between compositional domains, and therefore the majority of biotite is interpreted to be retrograde. At temperatures near the biotite-out boundary, the absence of orthopyroxene provides a lower pressure constraint of 5–5.5 kbar (Fig. 7a). The sample is modelled to contain 33–34 mol% magnetite and hematite, consistent with the high proportion of Fe-oxide minerals observed in this sample (~30 vol.%; Fig. 3c).

5.3.2. Sample IRD204-29

The peak metamorphic assemblage is interpreted as garnet, plagioclase, K-feldspar, cordierite, magnetite, hematite, sillimanite (occurring as inclusions in cordierite, along grain boundaries with cordierite and as sillimanite–magnetite–hematite aggregates), quartz and silicate melt. This assemblage occurs over a wide range of conditions, from pressures of ~2.6–6.8 kbar and temperatures in excess of 770 °C (Fig. 7b). Biotite in this sample is not interpreted to be part of the peak assemblage. The peak field for this sample is modelled to contain 18–19 mol% magnetite and hematite, in approximately equal proportions (Fig. 7b), consistent with the quantity of magnetite and hematite in observed in the rock (15–18 vol.%; Fig. 3d).

5.3.3. Sample IRD190-10A2

The peak metamorphic assemblage is interpreted as garnet, plagioclase, K-feldspar, cordierite, magnetite, hematite, quartz and silicate melt. The presence of cordierite and absence of sillimanite, except as inclusions in cordierite, suggests pressures were below 6.8 kbar (Fig. 7c). Biotite occurs as randomly oriented, anhedral flakes associated with magnetite–hematite as well as elongate grains that define the foliation in some parts of the sample, together with elongate magnetite–hematite. The ambiguity in the textural interpretation of biotite means that temperatures for the peak assemblage are poorly constrained. However, the general paucity of biotite in this sample (Fig. 3e) suggests that peak temperatures were near the biotite-out boundary, at 815–830 °C (Fig. 7c). The amount of magnetite modelled in the peak field in this sample (either with or without biotite) is 15–16.5 mol%, whereas the amount of hematite is <1 mol%. The sample contains 13 vol.% Fe-oxides (Fig. 3e) with magnetite the dominant oxide, consistent with the modelling.

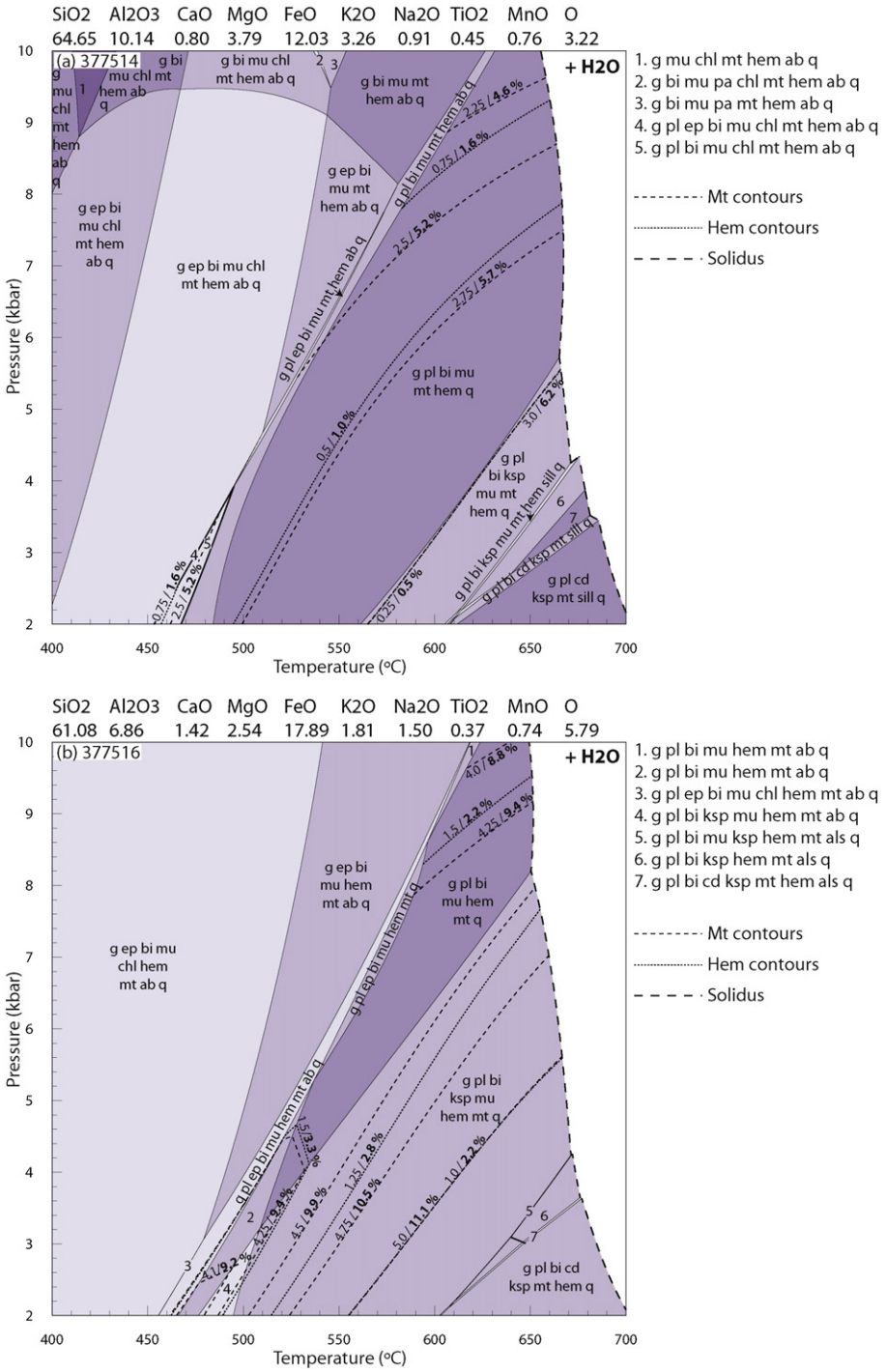

Fig. 6. *P–T* pseudosections for the Price Metasediments. The composition in mol% is given above each pseudosection. The pseudosections have been calculated with H_2O in excess. The bold dashed line is the solidus. The interpreted peak fields have been contoured for modal proportion of magnetite and hematite (in mol%). The higher number (bold text) is the absolute proportion of magnetite and hematite, excluding free water as a phase. The second number (regular text) is the proportion of magnetite and hematite calculated with free water as a phase. a) Sample 377514. b) Sample 377516.

5.4. Overall P–T evolution and conditions of the Price Metasediments–Warramboo system

The modelling of the Price Metasediments suggests metamorphism reached temperatures of ~460–470 °C. Peak pressures are poorly constrained but were less than 4 kbar (Fig. 6). This corresponds to an overall thermal gradient in excess of 115 °C/kbar. The mineral assemblages in the Warramboo gneisses occur over a large range of *P–T* conditions, but peak conditions are interpreted to be 830–850 °C and 5–6.8 kbar (Fig. 7), corresponding to a similar thermal gradient in excess of 120 °C/kbar. The prograde *P–T* path of the Warramboo gneisses is not well defined. The presence of aligned sillimanite inclusions in cordierite in several samples, together with the observation that cordierite contains inclusions of magnetite, hematite and garnet, suggests that the earlier evolution may have occurred outside the cordierite stability field and therefore involved higher pressures and/or lower temperatures (Fig. 7). The similar thermal gradient throughout the Warramboo–Price Metasediment system suggests a prograde evolution that necessarily

involved increasing temperatures with increasing crustal depth. However, any quantitative inferences about the prograde history are necessarily poorly constrained because the current residual bulk composition of the rock is not appropriate for modelling the prograde history (e.g. Johnson and White, 2011; Kelsey and Hand, 2015; Korhonen et al., 2013; White and Powell, 2002). The difficulty in constraining the

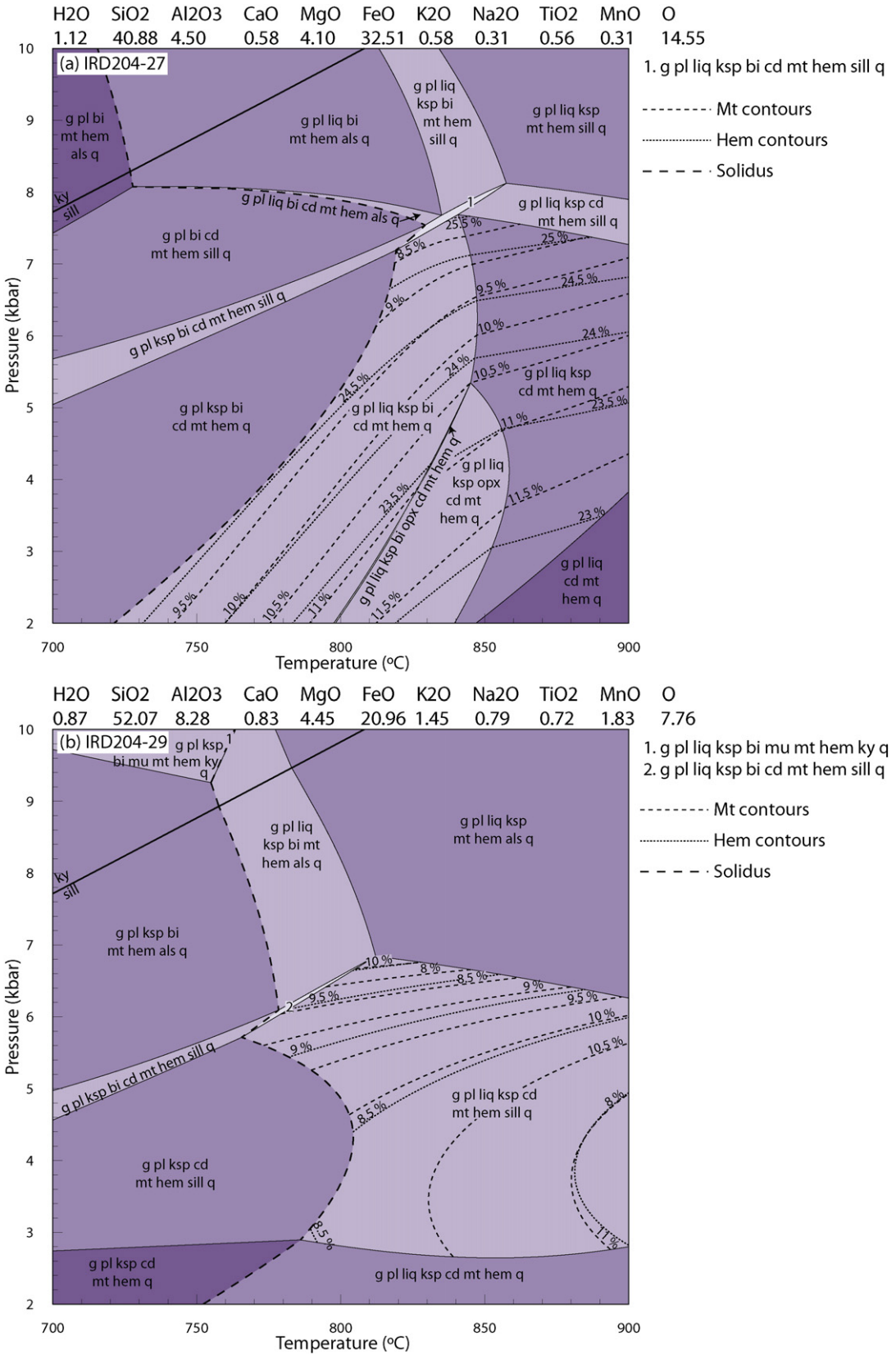

Fig. 7. *P–T* pseudosections of the Warramboo gneisses. The composition in mol% is given above each pseudosection. The solidus is denoted by a bold, dashed line. The interpreted peak fields are contoured for the proportion of magnetite and hematite (in mol%). a) Sample IRD204-27. b) Sample IRD204-29. c) Sample IRD190-10A2.

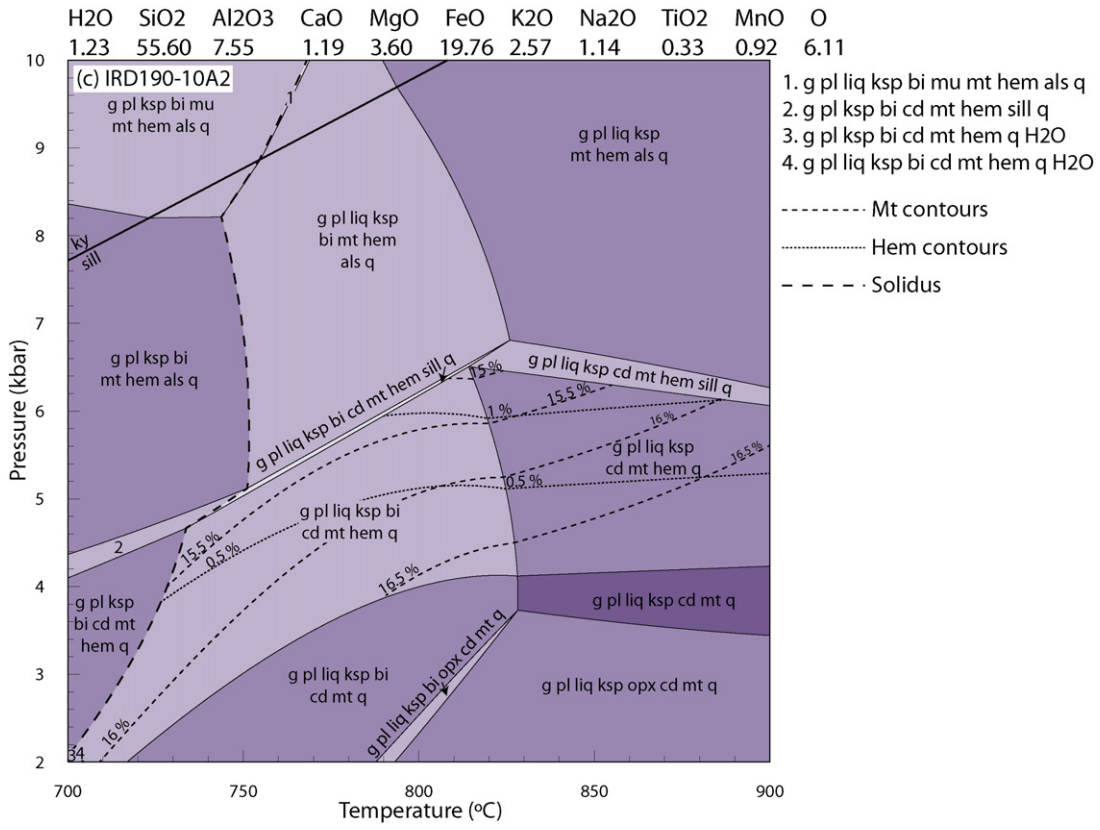

Fig. 7 (*continued*).

prograde history, combined with the high thermal gradient that involves large changes in temperature relative to pressure, means that for the purposes of modelling melt loss we have assumed a (simplified) isobaric heating path. A pressure of 6 kbar is used for the isobaric heating path, so that it intersected the interpreted peak conditions of the Warramboo deposit (Fig. 7).

5.5. Modelling the effects of prograde metamorphism and melt loss using the Price Metasediments

Forward modelling in a closed (i.e. isochemical) system using the compositions of the samples of Price Metasediments suggests that they are capable of producing the magnetite–cordierite–K-feldspar-bearing assemblages observed in the Warramboo gneisses at conditions similar to those inferred for the Warramboo deposit (Figs. 8a, 9a). However, the amount of melt modelled to be present in these assemblage fields in the closed system situation is ~50 mol% (Figs. 8a, 9a), which is rheologically impossible. Instead, melt was likely to have been lost via a series of melt loss events during prograde metamorphism. Three melt loss events were modelled to occur; the first is just up-temperature of the wet solidus, and the second and third are just up-temperature of the terminal muscovite and biotite breakdown-reactions where large volumes of melt are produced over a small temperature interval (shown as stars in Figs. 8, 9; Clemens, 2006; Redler et al., 2013; White and Powell, 2002). Melt loss events were modelled by removing all but 1 mol% of melt (interpreted to be the amount of melt retained on grain boundaries; Holness and Sawyer, 2008). After the removal of melt, another *P–T* pseudosection was calculated using the new composition (Table 1; Figs. 8b–d, 9b–d). This procedure was repeated after each melt loss event.

There are minor mismatches between the positions of some reaction boundaries in the subsolidus versus suprasolidus forward models, due to differences in the subsolidus and suprasolidus magnetite *a–x* models (White et al., 2002; White et al., 2000; White et al., 2014b). These differences prevent a direct comparison of the modal proportions of magnetite and hematite between the subsolidus and suprasolidus modelling. Importantly however, the effect of episodic melt loss on the modal proportions of these minerals at the interpreted peak conditions can be directly compared (Figs. 8–9). The bulk compositions and proportion of melt removed after each melt loss event are summarised in Table 1.

5.5.1. Sample 377514

At the peak conditions inferred for the Warramboo deposit, the total amount of melt that can be produced using the composition of 377514 in a closed system is ~50–65 mol% (Fig. 8a). However, if melt is removed episodically along the prograde evolution when the rock crosses the terminal H_2O, muscovite and biotite boundaries, the total cumulative amount of melt that can be produced by the time the rock reaches the interpreted peak conditions is 35–40 mol% (Table 1; Fig. 8d). At the interpreted peak conditions, the original 'closed system' composition of sample 377514 produces 6–7 mol% magnetite and 1–1.5 mol% hematite (Fig. 8a). After three melt loss events, approximately 35 mol% melt is modelled to have been removed from the composition (Table 1). The resulting amount of magnetite modelled to be present at the peak conditions increases to 8.5–10.5% and the amount of hematite increases to 1.5–2.5 mol% (Fig. 8d). Therefore, at the peak metamorphic conditions for the Warramboo deposit, sample 377514 shows a relative increase in total Fe-oxides from 7.5–8 mol% to 11.5–12 mol% as a result of three melt loss events, equivalent to a relative increase of ~35%. The relative amount of $Fe_2O_{3(TOTAL)}$ in the bulk composition increases by 35%, from 14.48 to 19.59 wt.% (Table 1).

5.5.2. Sample 377516

At the interpreted peak conditions of the Warramboo deposit, the amount of melt that can be produced in a closed system using the original

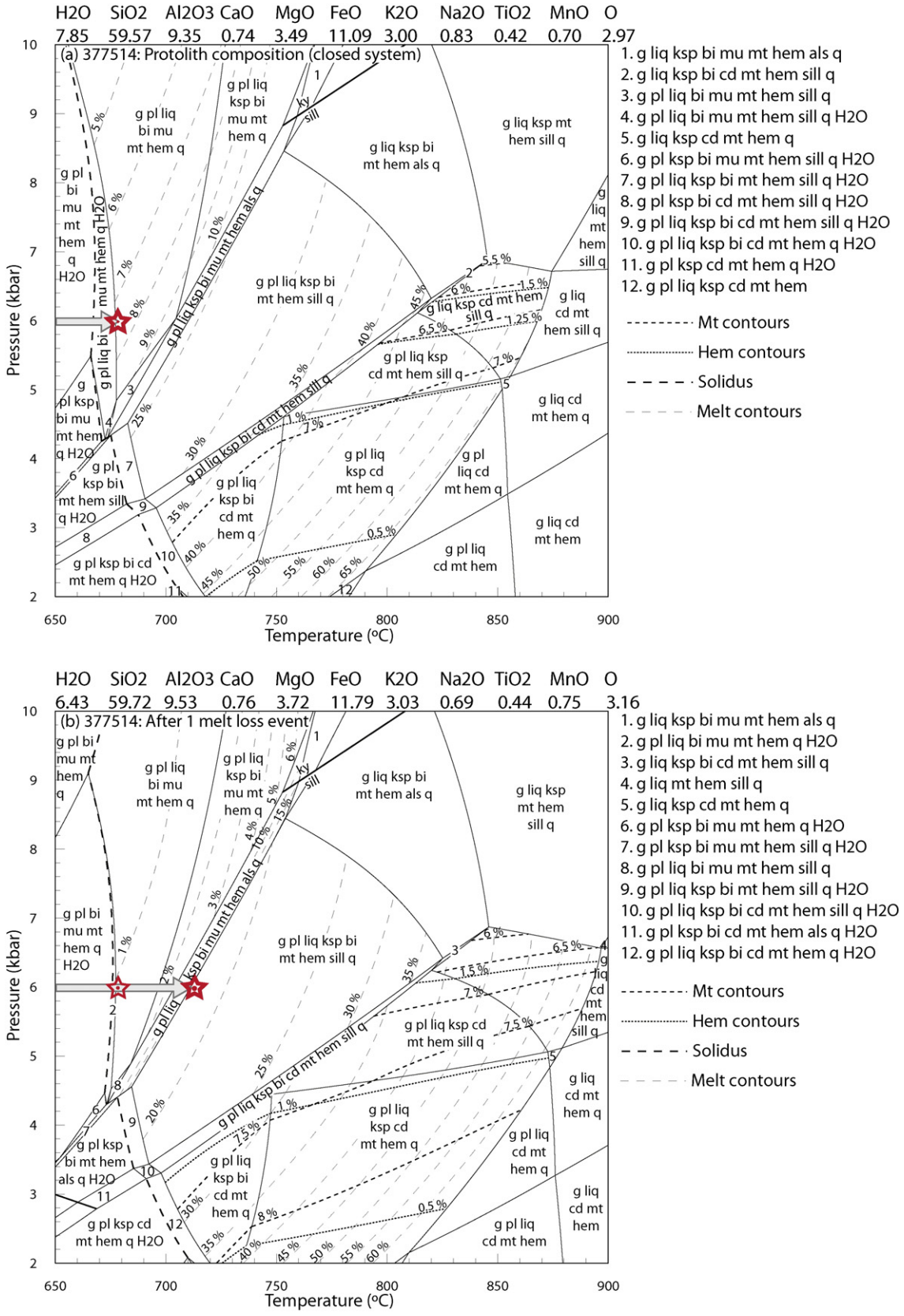

Fig. 8. *P–T* pseudosections modelling melt loss events for sample 377514. The composition in mol% is given above each pseudosection. The bold dashed line is the solidus, whereas the fine dashed lines represent contours of modal proportion of melt. The interpreted peak fields are contoured for the modal proportion of magnetite and hematite (in mol%). The grey arrow is the inferred isobaric heating path at 6 kbar and the stars mark the *P–T* conditions of each melt loss event. a) Closed system situation (no melt loss) using the original composition; b) after one melt loss event; c) after two melt loss events; d) after three melt loss events.

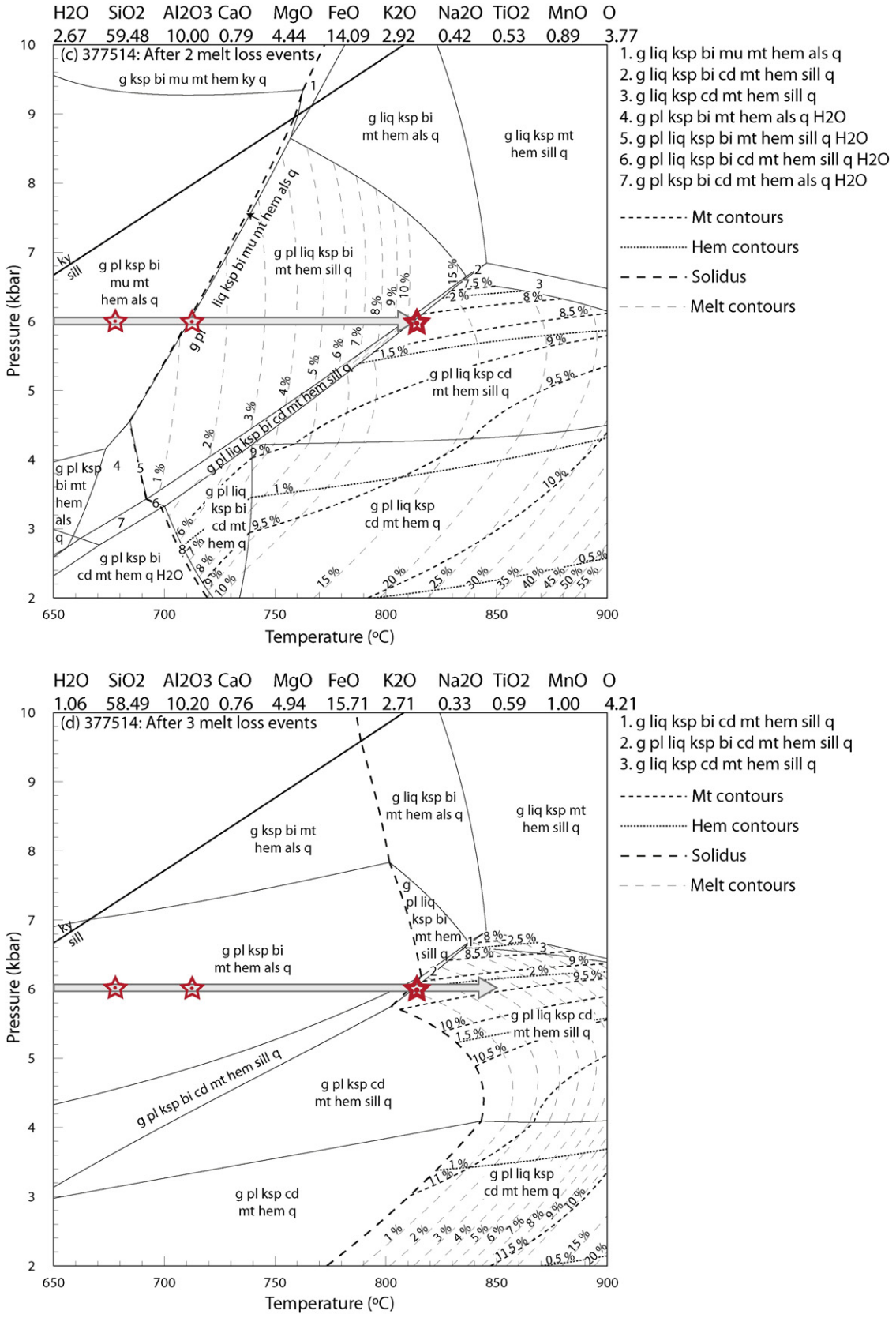

Fig. 8 (*continued*).

composition of sample 377516 is ~30–40 mol% (Fig. 9a). The original 'closed system' composition is modelled to produce 12.5–13.5 mol% magnetite and ~1.25–2 mol% hematite at peak conditions (Fig. 9a). After three melt loss events, approximately 19 mol% melt has been removed from the composition and the amount of magnetite and hematite modelled to be present at the peak conditions increases to 15.5–16.5 mol% and

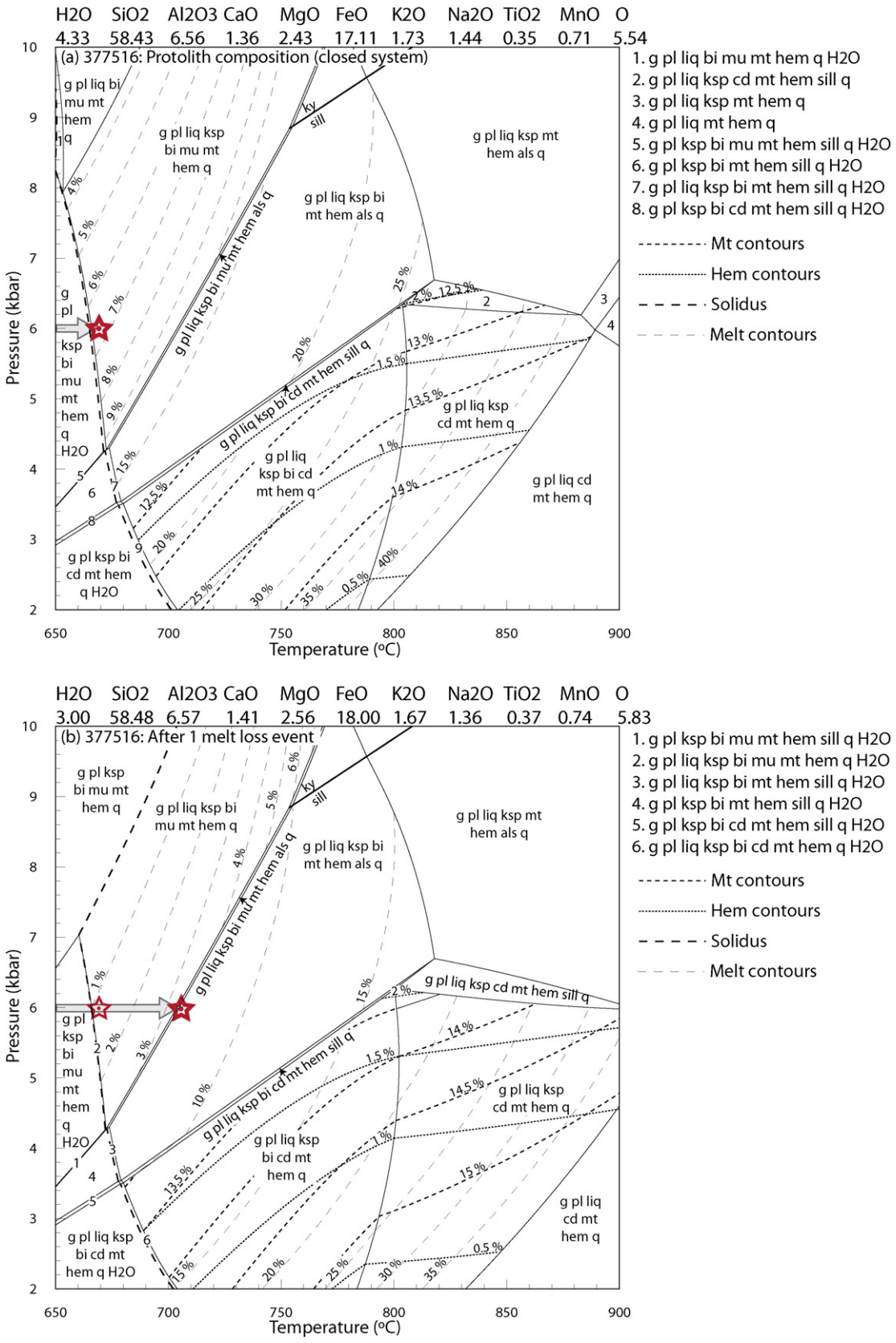

Fig. 9. *P–T* pseudosections modelling melt loss events for sample 377516. The composition in mol% is given above each pseudosection. The bold dashed line is the solidus, whereas the fine dashed lines represent contours of modal proportion of melt. The interpreted peak fields are contoured for the modal proportion of magnetite and hematite (in mol%). The grey arrow is the inferred isobaric heating path at 6 kbar and the stars mark the *P–T* conditions of each melt loss event. a) Closed system situation (no melt loss) using the original composition; b) after one melt loss event; c) after two melt loss events; d) after three melt loss events.

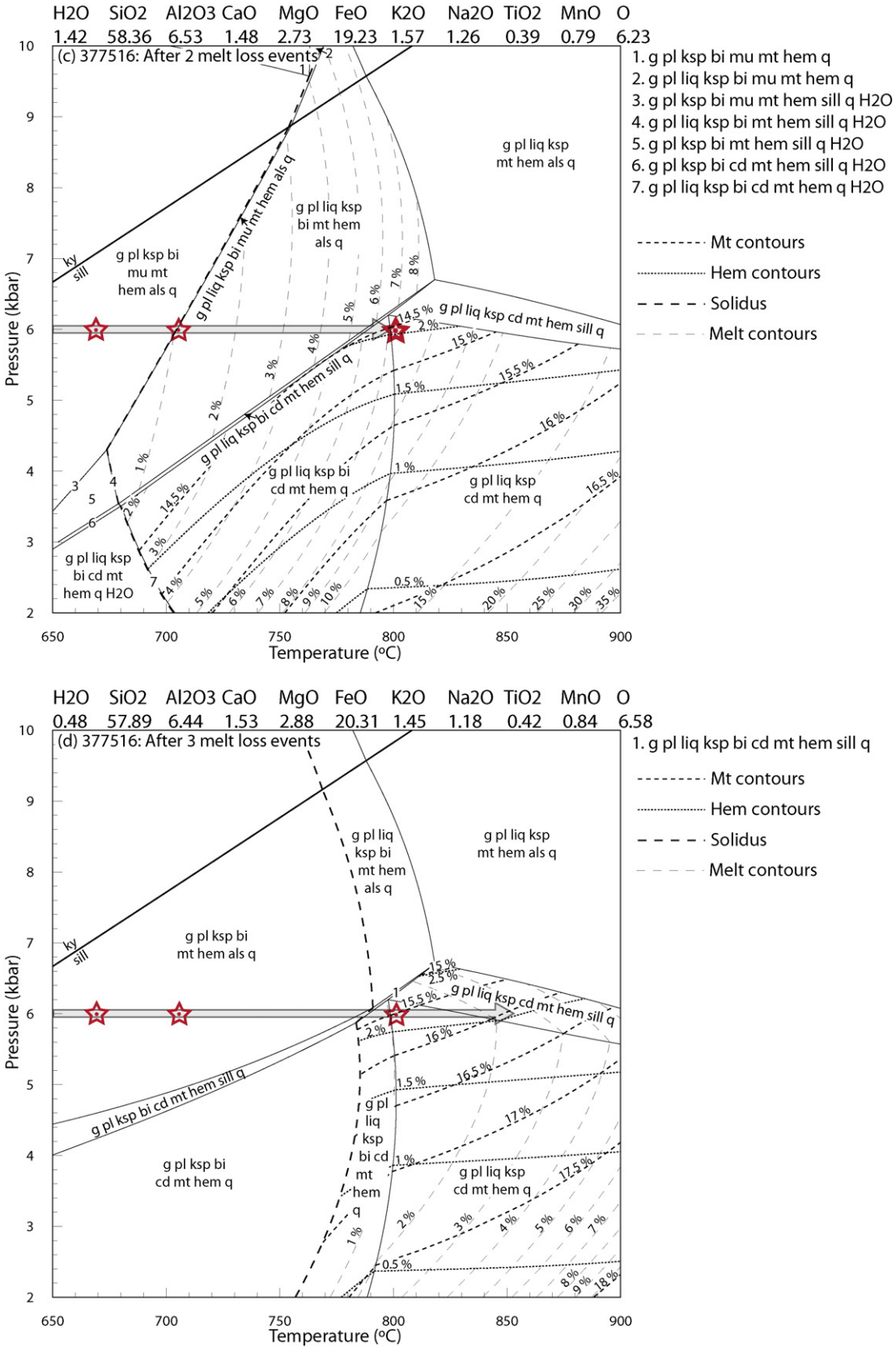

Fig. 9 (*continued*).

1.5–2.5 mol% respectively (Fig. 9d). Therefore, sample 377516 is modelled to show an increase in the total amount of Fe-oxides at peak conditions from ~14–14.5 mol% to ~18 mol% as a result of melt loss, equivalent to an increase of ~25%. The relative amount of $Fe_2O_{3(TOTAL)}$ in the bulk composition increases 16%, from 22.47 to 26.10 wt.% (Table 1).

6. Discussion

6.1. Implications for the generation of magnetite ore during metamorphism

Both the Price Metasediments and Warramboo magnetite-bearing gneisses display compositional heterogeneity on the metre to millimetre scale (Fig. 3). Therefore, the variation in iron oxide amounts in the Warramboo and Hambidge samples is likely to relate to differences in composition inherited from the original protoliths. The modelling suggests that the amount of $Fe_2O_{3(TOTAL)}$ in the bulk composition of the relatively iron-rich, muscovite-poor sample of Price Metasediments (sample 377516) can be increased by melt loss to values similar to samples IRD190-10A2 and IRD204-29 (in the range 25–27 wt.% $Fe_2O_{3(TOTAL)}$; Table 1). This provides support for the inference that the magnetite gneisses at Warramboo are correlatives of the Price Metasediments (Lane et al., 2015), and suggest that granulite facies metamorphism is a plausible mechanism to significantly upgrade sub-economic iron occurrences.

Metasedimentary rocks such as the Price Metasediments–Warramboo system are likely to contain interbedded pelitic and iron-rich psammitic layers, which together comprise the overall resource. Price Metasediments sample 377514 is modelled to cumulatively produce more melt during metamorphism to ~850 °C than sample 377516 (35 mol% compared to 19 mol%; Table 1). The larger volume of melt in sample 377514 reflects its higher proportion of muscovite (e.g. Brown, 2010; Patiño Douce and Harris, 1998; Vielzeuf and Holloway, 1988; White and Powell, 2002) compared to sample 377516. Sample 377514 also shows a more significant increase in the amount of $Fe_2O_{3(TOTAL)}$ in the bulk composition, with melt loss able to increase the amount of $Fe_2O_{3(TOTAL)}$ in the melt-depleted residuum by ~35%, as opposed to ~16% for the less melt-fertile sample 377516 (Fig. 10; Table 1). Packages that are originally rich in iron and more psammitic such as sample 377516 produce less melt than more pelitic compositions at any fixed temperature, and therefore experience a less significant increase in $Fe_2O_{3(TOTAL)}$ in the melt-depleted residuum. Therefore, the modelling suggests that whereas melt loss may not significantly enrich the horizons that were already enriched in iron but comparatively deficient in mica, melt loss from the more pelitic layers serves to improve iron contents in what would otherwise (at low metamorphic grades) have been very low value parts of the deposit system, thereby improving the overall size of the resource.

Metamorphism is also a mechanism to increase the abundance of Fe-oxide minerals by increasing temperatures. Figs. 8 and 9 illustrate the increasing proportion of magnetite and hematite at peak conditions, as a function of changing composition. Fig. 10 illustrates the combined effect of prograde heating from 650 to 850 °C and melt loss on the proportion of the phases and the amount of total iron ($Fe_2O_{3(TOTAL)}$) in the melt-depleted rock. It suggests that increasing temperature as well as compositional changes as a result of melt loss both play a role in increasing the proportion of iron oxides. The effect of both isobaric heating and melt loss in sample 377514 is to significantly increase the sum amount of magnetite and hematite from 6.1 to 11.6 mol% (Fig. 10a), whereas the sum amount of magnetite and hematite in sample 377516 increases from 13.1 to 18.5 mol% (Fig. 10b). In addition, high-grade metamorphism will typically increase grain size, improving crushing and concentration processes.

6.2. Limitations of the modelling

One of the main limitations of the *P–T* modelling discussed above is that some of the components commonly occurring in natural rocks, such as ZnO, Cr_2O_3 and P_2O_5, cannot be effectively modelled in the currently available thermodynamic system. The whole rock chemistry shows that the samples in this study are also rich in MnO (0.37–2.06 wt.%; Table 1). The current Mn-bearing activity–composition (*a–x*) models have been developed for metapelitic rocks containing typical amounts of MnO (<0.3 wt.%), and therefore they may not be reliable for the MnO-rich rocks in this study (White et al., 2014b). The *a–x* models for hematite, garnet, cordierite, and biotite (and chlorite, subsolidus) incorporate Mn, and in particular, Mn exerts an important influence on the stability of garnet (e.g. Boger and Hansen, 2004; Johnson et al., 2003; Mahar et al., 1997; Tinkham and Ghent, 2005; Tinkham et al., 2001; White et al., 2014b). However, the *a–x* model for magnetite does not incorporate Mn (White et al., 2002; White et al., 2000), and therefore modelling using the current *a–x* models may underestimate the amount of magnetite by artificially stabilising minerals such as garnet, which sequester Fe, in the calculations. In addition, both the Price Metasediments samples and sample IRD204-27 contain small amounts of apatite, which affects the calcium budget of the rock, but cannot be modelled in the MnNCKFMASHTO system (or any other system currently). The presence of abundant monazite in some samples means that the effect of apatite cannot be easily accounted for using the amount of P_2O_5 in the bulk composition. Therefore, this limitation may artificially stabilise Ca-bearing phases such as garnet and plagioclase in the calculations.

In applying the results specifically to the Price Metasediment–Warramboo system, there is some uncertainty in modelling melt loss as the prograde *P–T* path is poorly constrained, and therefore determining the number of likely melt loss 'events' is difficult. An isobaric heating path at 6 kbar was selected as a proxy for the 'flat' apparent thermal gradient recorded by the low- and high-temperature samples, as it intersected cordierite-bearing fields at the interpreted peak conditions. A different pressure evolution would produce slightly less melt at higher pressure and slightly more melt at lower pressure. The crossing of the wet solidus and the main hydrate breakdown reactions have been used as a proxy for melt loss events. In the case of the muscovite-breakdown reaction, this means that up to 19 mol% melt was modelled to be present in the rock prior to melt loss (Figs. 8, 9). However, in a static system, melt loss has been interpreted to occur when the melt connectivity threshold is exceeded, at ~7% melt (Rosenberg and Handy, 2005). In a system that is undergoing deformation, this threshold is likely to be much lower, and melt loss may even be continuous (e.g. Brown, 2010; Handy et al., 2001; Johnson et al., 2011). Therefore, due to the uncertainties in constraining the *P–T* path and the threshold of melt loss applicable to the Price Metasediment–Warramboo system, the modelling in this study is likely to underestimate the number of melt loss events. An increased number of melt loss events is likely to produce slightly less cumulative melt overall, as each melt loss event makes the remaining rock more residual and more difficult to melt (e.g. Brown, 2013; Vielzeuf et al., 1990; White and Powell, 2002). However, these uncertainties are not interpreted to significantly affect the relationship between melting and the proportion of iron in the residual rock.

6.3. Implications for exploration for magnetite-rich iron ore deposits

Most large magnetite deposits are interpreted to form as a result of primary igneous processes (e.g. Naslund et al., 2002; Nystroem and Henriquez, 1994), deposition of iron oxides as a result of secondary hydrothermal processes (e.g. Dare et al., 2015; Kalczynski and Gates, 2014; Puffer and Gorring, 2005; Sillitoe and Burrows, 2002), or a combination of the two (Knipping et al., 2015). There are comparatively few examples of magnetite deposits analogous to the Warramboo deposit, where mineralisation is hosted in a Fe-rich, clastic sediment (e.g. Lupulescu et al., 2014; Mücke, 2005; Palmer, 1970; Tyler et al., 2014). However, recognition of this deposit type may have important implications for iron ore exploration in high temperature (>650–700 °C) metamorphic terranes that have undergone partial melting. Similar magnetite deposits that are hosted in granulite facies metasedimentary rocks include the Benson Mine in the Grenville Orogen (Lupulescu et al., 2014; Palmer, 1970) and the Southdown magnetite deposit in the Albany–Fraser Orogen in Western Australia (Tyler et al., 2014). The Benson Mine was proposed to have formed by

metamorphism of pelitic sediment (Lupulescu et al., 2014; Palmer, 1970). Although there are no modern metamorphic *P–T* constraints, the surrounding rocks have been migmatised (Palmer, 1970) suggesting that combined metamorphism and melt loss may have been the mechanism for creating and upgrading this deposit. Similarly, the Southdown magnetite deposit is hosted in granulite facies gneisses and has been interpreted to have been an Fe-rich sediment that experienced two phases of high temperature metamorphism (Tyler et al., 2014).

Therefore, the combination of increased grain size and increased Fe-oxide contents linked to melt loss makes high-temperature metamorphic terranes attractive targets for magnetite-dominated iron ore deposits. The modelling suggests that the proportion of magnetite to hematite increases towards higher temperatures and lower pressures (Figs. 7–9). Therefore, low pressure, high temperature terranes may be more prospective for magnetite-dominated rather than hematite-dominated iron ore deposits. Combining regional geophysical techniques such as aeromagnetic imagery with an understanding of the

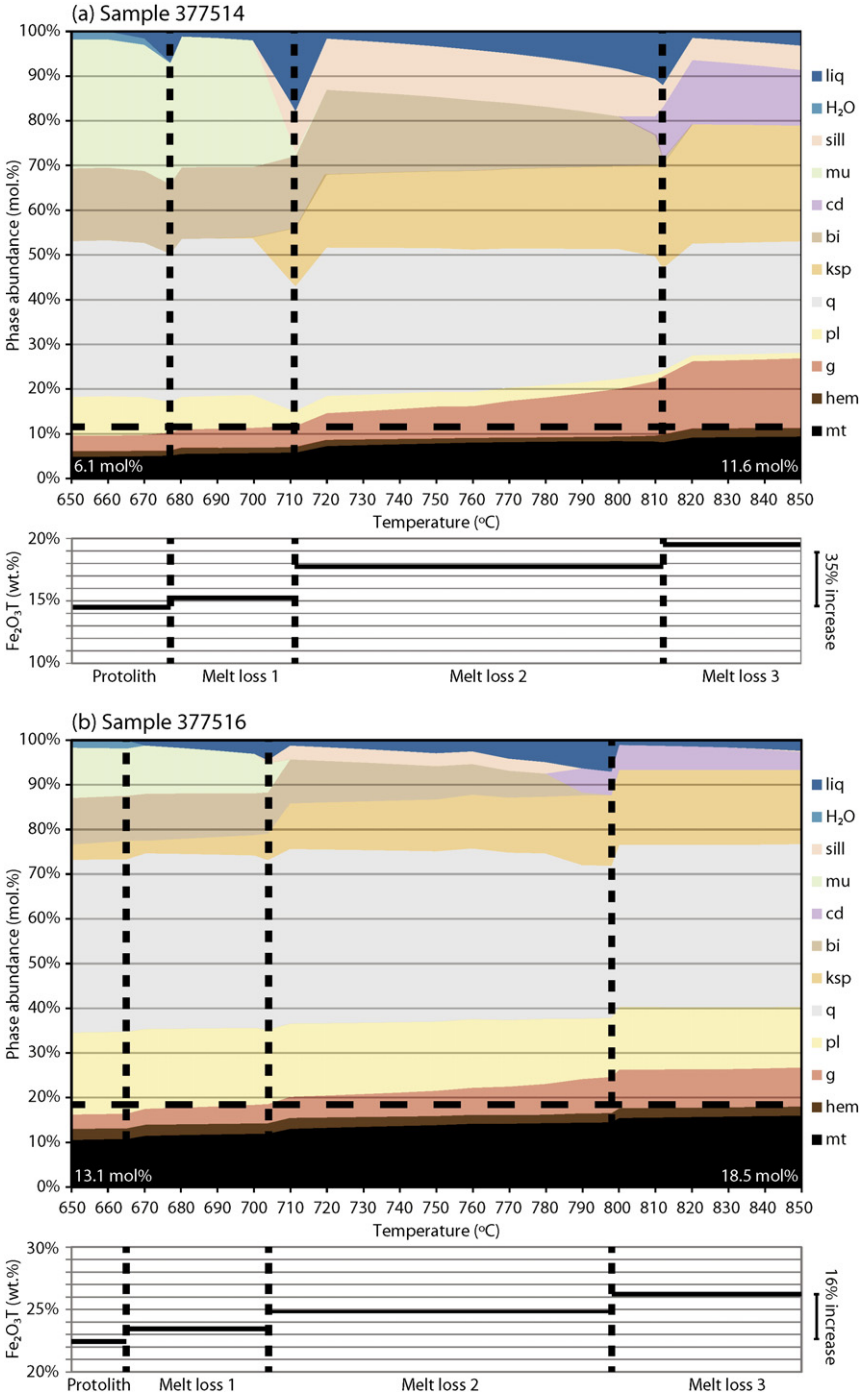

Fig. 10. Change in mole proportion of phases as a function of temperature and melt loss along a prograde isobaric heating path from 650 to 850 °C. The vertical bold dashed lines represent melt loss events. The white numbers give the total abundance of magnetite and hematite in mol%, and the horizontal dashed line illustrates the increased abundance along the isobaric heating path. The amount of $Fe_2O_{3(TOTAL)}$ in the bulk composition along the prograde path for each sample is shown below. a) Sample 377514. b) Sample 377516.

metamorphic conditions of a terrane (particularly with respect to the melting and melt loss history) may be a powerful tool for exploration.

7. Conclusions

Phase equilibria forward modelling suggests that melt loss associated with progressive metamorphism, culminating in granulite facies conditions is a mechanism to enrich the Fe-oxide content of metasedimentary rocks. The specific extent of enrichment is controlled by the melt fertility of the rock. For the Price Metasediments, the combined effect of metamorphism and melt loss from muscovite-rich horizons with more melt-fertile compositions increases the total amount of Fe-oxides from ~6 mol% to 11.5 mol%, equivalent to a relative increase of ~90%. The relative amount of $Fe_2O_{3(TOTAL)}$ in the bulk composition increases by ~35% as a result of melt loss. More Fe-rich, muscovite-poor horizons produce less melt and therefore do not show the same increase, with the total amount of Fe-oxides increasing ~40%, from 13 mol% to ~18.5 mol%, and the relative amount of $Fe_2O_{3(TOTAL)}$ in the bulk composition increases 16%. Varying the oxidation state of a rock does not significantly affect the amount of Fe-oxides at granulite facies, but it does affect the proportion of magnetite to hematite. The results of this work suggest that melt loss is a realistic mechanism to improve the overall ore grade within metamorphic iron ore deposits.

Acknowledgements

Stan Mertzman is thanked for the geochemical analyses. Chris Yakymchuck and Tim Johnson are thanked for their constructive reviews. Iron Road is thanked for providing the samples for this study. Iron Road and the Geological Survey of South Australia are thanked for providing funding. This manuscript forms TRaX record # 337. RAD publishes with the permission of the Director, Geological Survey of South Australia.

Appendix 1. Whole rock geochemistry (in wt.%).

Sample	773514	773516	IRD204-27	IRD204-29	190-10A2
SiO2	58.19	57.54	41.51	49.71	52.75
TiO2	0.54	0.46	0.76	0.91	0.41
Al2O3	15.49	10.97	7.74	13.42	12.15
Fe2O3	10.88	19.45	39.27	19.69	15.40
FeO	3.16	2.65	4.15	6.22	8.56
MnO	0.81	0.82	0.37	2.06	1.03
MgO	2.29	1.61	2.79	2.85	2.29
CaO	0.67	1.25	0.55	0.74	1.06
Na2O	0.84	1.46	0.33	0.77	1.12
K2O	4.60	2.67	0.92	2.17	3.82
P2O5	0.18	0.33	0.34	0.19	0.22
LOI	2.32	1.28	0.85	1.18	0.86
Total	99.97	100.49	99.58	99.90	99.67

References

Boger, S.D., Hansen, D., 2004. Metamorphic evolution of the Georgetown Inlier, northeast Queensland, Australia; evidence for an accreted Palaeoproterozoic terrane? J. Metamorph. Geol. 22, 511–527.

Boger, S.D., White, R.W., Schulte, B., 2012. The importance of iron speciation (Fe + 2/Fe + 3) in determining mineral assemblages: an example from the high-grade aluminous metapelites of southeastern Madagascar. J. Metamorph. Geol. 30, 997–1018.

Brown, M., 2010. The spatial and temporal patterning of the deep crust and implications for the process of melt extraction. Phil. Trans. R. Soc. A 368, 11–51.

Brown, M., 2013. Granite: from genesis to emplacement. Geol. Soc. Am. Bull. 125, 1079–1113.

Clemens, J.D., 2006. Melting of the continental crust: fluid regimes, melting reactions, and source-rock fertility. In: Brown, M., Rushmer, T. (Eds.), Evolution and Differentiation of the Continental Crust. Cambridge University Press, Cambridge, pp. 297–331.

Clemens, J.D., Vielzeuf, D., 1987. Constraints on melting and magma production in the crust. Earth Planet. Sci. Lett. 86, 287–306.

Cutts, K., Hand, M., Kelsey, D.E., 2011. Evidence for early Mesoproterozoic (ca. 1590 Ma) ultrahigh-temperature metamorphism in southern Australia. Lithos 124, 1–16.

Cutts, K.A., Kelsey, D.E., Hand, M., 2013. Evidence for late Paleoproterozoic (ca 1690–1665 Ma) high- to ultrahigh-temperature metamorphism in southern Australia: implications for Proterozoic supercontinent models. Gondwana Res. 23, 617–640.

Daly, S.J., Fanning, C.M., Fairclough, M.C., 1998. Tectonic evolution and exploration potential of the Gawler Craton, South Australia. AGSO J. Aust. Geol. Geophys. 17, 145–168.

Dare, S.S., Barnes, S.-J., Beaudoin, G., 2015. Did the massive magnetite "lava flows" of El Laco (Chile) form by magmatic or hydrothermal processes? New constraints from magnetite composition by LA-ICP-MS. Mineral. Deposita 50, 607–617.

Deer, W.A., Howie, R.A., Zussman, J., 1992. An Introduction to the Rock-Forming Minerals. 2nd edition. Longman, United Kingdom.

Diener, J.F.A., Powell, R., 2010. Influence of ferric iron on the stability of mineral assemblages. J. Metamorph. Geol. 28, 599–613.

Diener, J.F.A., White, R.W., Powell, R., 2008. Granulite facies metamorphism and subsolidus fluid-absent reworking, Strangways Range, Arunta Block, central Australia. J. Metamorph. Geol. 26, 603–622.

Droop, G.T.R., Clemens, J.D., Dalrymple, D.J., 2003. Processes and conditions during contact anatexis, melt escape and restite formation: the Huntly Gabbro Complex, NE Scotland. J. Petrol. 44, 995–1029.

Dutch, R., Hand, M., Kinny, P.D., 2008. High-grade Paleoproterozoic reworking in the southeastern Gawler Craton, South Australia. Aust. J. Earth Sci. 55, 1063–1081.

Dutch, R.A., Hand, M., Kelsey, D.E., 2010. Unravelling the tectonothermal evolution of reworked Archean granulite facies metapelites using in situ geochronology: an example from the Gawler Craton, Australia. J. Metamorph. Geol. 28, 293–316.

Fanning, C.M., Flint, R.B., Parker, A.J., Ludwig, K.R., Blissett, A.H., 1988. Refined Proterozoic evolution of the Gawler Craton, South Australia, through U–Pb zircon geochronology. Precambrian Res. 40–41, 363–386.

Fanning, C.M., Reid, A.J., Teale, G.S., 2007. A geochronological framework for the Gawler Craton, South Australia. Bull. Geol. Surv. S. Aust. 55.

Forbes, C.J., Giles, D., Jourdan, F., Sato, K., Omori, S., Bunch, M., 2012. Cooling and exhumation history of the northeastern Gawler Craton, South Australia. Precambrian Res. 200–203, 209–238.

Fraser, G., McAvaney, S., Neumann, N., Szpunar, M., Reid, A., 2010. Discovery of early Mesoarchean crust in the eastern Gawler Craton, South Australia. Precambrian Res. 179, 1–21.

Hand, M., Reid, A.J., Jagodzinski, E., 2007. Tectonic framework and evolution of the Gawler Craton, Southern Australia. Econ. Geol. 102, 1377–1395.

Handy, M.R., Mulch, A., Rosenau, M., Rosenberg, C.L., 2001. The role of fault zones and melts as agents of weakening, hardening and differentiation of the continental crust: a synthesis. Geol. Soc. Lond., Spec. Publ. 186, 305–332.

Holland, T.J.B., Powell, R., 2011. An improved and extended internally consistent thermodynamic dataset for phases of petrological interest, involving a new equation of state for solids. J. Metamorph. Geol. 29, 333–383.

Holness, M.B., Sawyer, E.W., 2008. On the pseudomorphing of melt-filled pores during the crystallization of migmatites. J. Petrol. 49, 1343–1363.

Howard, K.E., Hand, M., Barovich, K.M., Payne, J.L., Belousova, E.A., 2011a. U–Pb, Lu–Hf and Sm–Nd isotopic constraints on provenance and depositional timing of metasedimentary rocks in the western Gawler Craton: implications for Proterozoic reconstruction models. Precambrian Res. 184, 43–62.

Howard, K.E., Hand, M., Barovich, K.M., Payne, J.L., Cutts, K.A., Belousova, E.A., 2011b. U–Pb zircon, zircon Hf and whole-rock Sm–Nd isotopic constraints on the evolution of Paleoproterozoic rocks in the northern Gawler Craton. Aust. J. Earth Sci. 58, 615–638.

IronRoad, 2014. Presentation: Central Eyre Iron Project — Our Technical Journey. http://www.ironroadlimited.com.au/images/files/presentations/20141029%20IRD%20CEIP%20Our%20Journey%20.pdf.

Johnson, T.E., White, R.W., 2011. Phase equilibrium constraints on conditions of granulite-facies metamorphism at Scourie, NW Scotland. J. Geol. Soc. 168, 147–158.

Johnson, T.E., Brown, M., Solar, G.S., 2003. Low–pressure subsolidus and suprasolidus phase equilibria in the MnNCKFMASH system: constraints on conditions of regional metamorphism in western Maine, northern Appalachians. Am. Mineral. 88, 624–638.

Johnson, T.E., White, R.W., Brown, M., 2011. A year in the life of an aluminous metapelite xenolith—the role of heating rates, reaction overstep, H_2O retention and melt loss. Lithos 124, 132–143.

Johnson, T.E., White, R.W., Powell, R., 2008. Partial melting of metagreywacke: a calculated mineral equilibria study. J. Metamorph. Geol. 26, 837–853.

Kalczynski, M.J., Gates, A.E., 2014. Hydrothermal alteration, mass transfer and magnetite mineralization in dextral shear zones, western Hudson Highlands, New York, United States. Ore Geol. Rev. 61, 226–247.

Kelsey, D.E., Hand, M., 2015. On ultrahigh temperature crustal metamorphism: phase equilibria, trace element thermometry, bulk composition, heat sources, timescales and tectonic settings. Geosci. Front. 6, 311–356.

Knipping, J.L., Bilenker, L.D., Simon, A.C., Reich, M., Barra, F., Deditius, A.P., Lundstrom, C., Bindeman, I., Munizaga, R., 2015. Giant Kiruna-type deposits form by efficient flotation of magmatic magnetite suspensions. Geology 43, 591–594.

Korhonen, F.J., Brown, M., Clark, C., Bhattacharya, S., 2013. Osumilite–melt interactions in ultrahigh temperature granulites: phase equilibria modelling and implications for the P–T–t evolution of the Eastern Ghats Province, India. J. Metamorph. Geol. 31, 881–907.

Korhonen, F.J., Saito, S., Brown, M., Siddoway, C.S., 2010. Modeling multiple melt loss events in the evolution of an active continental margin. Lithos 116, 230–248.

Lane, K., Jagodzinski, E.A., Dutch, R., Reid, A.J., Hand, M., 2015. Age constraints on the timing of iron ore mineralisation in the southeastern Gawler Craton. Aust. J. Earth Sci. 62, 55–75.

Lo Pò, D., Braga, R., 2014. Influence of ferric iron on phase equilibria in greenschist facies assemblages: the hematite-rich metasedimentary rocks from the Monti Pisani (Northern Apennines). J. Metamorph. Geol. 32, 371–387.

Lupulescu, M.V., Bailey, D.G., Hawkins, M., Carl, J.D., Chiarenzelli, J.R., 2014. The Benson Mines, St. Lawrence County, New York: history of the discovery, mining, and mineralogy of the deposit. Rocks Miner. 89, 118–131.
Mahar, E.M., Baker, J.M., Powell, R., Holland, T.J.B., Howell, N., 1997. The effect of Mn on mineral stability in metapelites. J. Metamorph. Geol. 15, 223–238.
McFarlane, C.R.M., 2006. Palaeoproterozoic evolution of the Challenger Au deposit, South Australia, from monazite geochronology. J. Metamorph. Geol. 24, 75–87.
McKay, A.D., Miezitis, Y., Porritt, K., Britt, A.F., Champion, D.C., Cadman, S., Towner, R., Summerfield, D., Whitaker, A., Huston, D., Jaireth, S., Sexton, M., Schofield, A., Hoatson, D., Senior, A.B., Carson, L., 2014. Australia's Identified Mineral Resources 2013. Geoscience Australia, Canberra, Australia.
Morrissey, L.J., Hand, M., Kelsey, D.E., 2015. Multi-stage metamorphism in the Rayner-Eastern Ghats Terrane: P–T–t constraints from the northern Prince Charles Mountains, east Antarctica. Precambrian Res. 267, 137–163.
Morrissey, L.J., Hand, M., Wade, B.P., Szpunar, M., 2013. Early Mesoproterozoic metamorphism in the Barossa Complex, South Australia: links with the eastern margin of Proterozoic Australia. Aust. J. Earth Sci. 60, 769–795.
Mücke, A., 2005. The Nigerian manganese-rich iron-formations and their host rocks—from sedimentation to metamorphism. J. Afr. Earth Sci. 41, 407–436.
Mudd, G.M., 2010. The environmental sustainability of mining in Australia: key mega-trends and looming constraints. Res. Policy 35, 98–115.
Naslund, H., Henríquez, F., Nyström, J., Vivallo, W., Dobbs, F., 2002. Magmatic iron ores and associated mineralization: examples from the Chilean High Andes and Coastal Cordillera. In: Porter, T.M. (Ed.), Hydrothermal Iron Oxide Copper–Gold and Related Deposits: A Global Perspective. PCG Publishing, Adelaide, Australia, pp. 207–226.
Nystroem, J.O., Henriquez, F., 1994. Magmatic features of iron ores of the Kiruna type in Chile and Sweden; ore textures and magnetite geochemistry. Econ. Geol. 89, 820–839.
Oliver, R.L., Fanning, C.M., 1997. Australia and Antarctica: Precise correlation of Palaeoproterozoic terrains. In: Ricci, C.A. (Ed.), The Antarctic Region: Geological Evolution and Processes. Terra Antartica Publication, Sienna.
Palmer, D.F., 1970. Geology and ore deposits near Benson mines, New York. Econ. Geol. 65, 31–39.
Patiño Douce, A.E., Harris, N., 1998. Experimental constraints on Himalayan anatexis. J. Petrol. 39, 689–710.
Payne, J.L., Barovich, K., Hand, M., 2006. Provenance of metasedimentary rocks in the northern Gawler Craton, Australia: implications for Palaeoproterozoic reconstructions. Precambrian Res. 148, 275–291.
Payne, J.L., Hand, M., Barovich, K.M., Reid, A., Evans, D.A.D., 2009. Correlations and reconstruction models for the 2500–1500 Ma evolution of the Mawson Continent. Geol. Soc. Lond., Spec. Publ. 323, 319–355.
Payne, J.L., Hand, M., Barovich, K.M., Wade, B.P., 2008. Temporal constraints on the timing of high-grade metamorphism in the northern Gawler Craton: implications for assembly of the Australian Proterozoic. Aust. J. Earth Sci. 55, 623–640.
Powell, R., Downes, J., 1990. Garnet porphyroblast-bearing leucosomes in metapelites: mechanisms, phase diagrams, and an example from Broken Hill, Australia. In: Brown, M. (Ed.), Ashworth, J.R. High-temperature Metamorphism and Crustal Anatexis, Springer Netherlands, pp. 105–123.
Powell, R., White, R.W., Green, E.C.R., Holland, T.J.B., Diener, J.F.A., 2014. On parameterizing thermodynamic descriptions of minerals for petrological calculations. J. Metamorph. Geol. 32, 245–260.
Puffer, J.H., Gorring, M.L., 2005. The Edison magnetite deposits in the context of pre-, syn-, and post-orogenic metallogenesis in the Grenville Highlands of New Jersey. Can. J. Earth Sci. 42, 1735–1748.
Redler, C., White, R.W., Johnson, T.E., 2013. Migmatites in the Ivrea Zone (NW Italy): constraints on partial melting and melt loss in metasedimentary rocks from Val Strona di Omegna. Lithos 175-176, 40–53.
Reid, A.J., Hand, M., 2012. Mesoarchean to Mesoproterozoic evolution of the southern Gawler Craton, South Australia. Episodes 35, 216–225.
Reid, A.J., Jagodzinski, E.A., Fraser, G.L., Pawley, M.J., 2014. SHRIMP U–Pb zircon age constraints on the tectonics of the n=Neoarchean to early Paleoproterozoic transition within the Mulgathing Complex, Gawler Craton, South Australia. Precambrian Res. 250, 27–49.
Rigby, M.J., Droop, G.T.R., 2011. Fluid-absent melting versus CO2 streaming during the formation of pelitic granulites: a review of insights from the cordierite fluid monitor. Mem. Geol. Soc. Am. 207, 39–60.
Rosenberg, C.L., Handy, M.R., 2005. Experimental deformation of partially melted granite revisited: implications for the continental crust. J. Metamorph. Geol. 23, 19–28.
Sawyer, E.W., 1994. Melt segregation in the continental crust. Geology 22, 1019–1022.
Sillitoe, R.H., Burrows, D.R., 2002. New field evidence bearing on the origin of the El Laco magnetite deposit, Northern Chile. Econ. Geol. 97, 1101–1109.
Swain, G., Barovich, K., Hand, M., Ferris, G., Schwarz, M., 2008. Petrogenesis of the St Peter Suite, southern Australia: arc magmatism and Proterozoic crustal growth of the South Australian Craton. Precambrian Res. 166, 283–296.
Swain, G., Woodhouse, A., Hand, M., Barovich, K., Schwarz, M., Fanning, C.M., 2005. Provenance and tectonic development of the late Archaean Gawler Craton, Australia; U–Pb zircon, geochemical and Sm–Nd isotopic implications. Precambrian Res. 141, 106–136.
Tinkham, D.K., Ghent, E.D., 2005. Estimating garnet growth P–T conditions with pseudosections and the problem of effective bulk composition. Can. Mineral. 43, 35–50.
Tinkham, D.K., Zuluaga, C.A., Stowell, H.H., 2001. Metapelite phase equilibria modeling in MnNCKFMASH: the effect of variable Al2O3 and MgO/(MgO + FeO) on mineral stability. Geol. Mater. Res. 3, 1–42.
Tyler, I.M., Spaggiari, C.V., Occhipinti, S.A., Kirkland, C.L., Smithies, H.R., 2014. The Albany–Fraser deep reflection seismic and MT survey: implications for mineral systems. In: Spaggiari, C.V., Tyler, I.M. (Eds.), Albany–Fraser Orogen seismic and Magnetotelluric (MT) Workshop 2014: Extended Abstracts. Geological Survey of Western Australia, pp. 174–182.
Vassallo, J.J., Wilson, C.J.L., 2002. Palaeoproterozoic regional-scale non-coaxial deformation: an example from eastern Eyre Peninsula, South Australia. J. Struct. Geol. 24, 1–24.
Vielzeuf, D., Holloway, J., 1988. Experimental determination of the fluid-absent melting relations in the pelitic system. Contrib. Mineral. Petrol. 98, 257–276.
Vielzeuf, D., Clemens, J.D., Pin, C., Moinet, E., 1990. In: Vielzeuf, D., Vidal, P. (Eds.), Granites, granulites, and crustal differentiation. Granulites and Crustal Evolution, Springer Netherlands, pp. 59–85.
White, R.W., Powell, R., 2002. Melt loss and the preservation of granulite facies mineral assemblages. J. Metamorph. Geol. 20, 621–632.
White, R.W., Powell, R., Clarke, G.L., 2002. The interpretation of reaction textures in Fe-rich metapelitic granulites of the Musgrave Block, central Australia: constraints from mineral equilibria calculations in the system K2O–FeO–MgO–Al2O3–SiO2–H2O–TiO2–Fe2O3. J. Metamorph. Geol. 20, 41–55.
White, R.W., Powell, R., Holland, T.J.B., 2001. Calculation of partial melting equilibria in the system Na2O–CaO–K2O–FeO–MgO–Al2O3–SiO2–H2O (NCKFMASH). J. Metamorph. Geol. 19, 139–153.
White, R.W., Powell, R., Holland, T.J.B., Johnson, T.E., Green, E.C.R., 2014a. New mineral activity–composition relations for thermodynamic calculations in metapelitic systems. J. Metamorph. Geol. 32, 261–286.
White, R.W., Powell, R., Holland, T.J.B., Worley, B.A., 2000. The effect of TiO2 and Fe2O3 on metapelitic assemblages at greenschist and amphibolite facies conditions: mineral equilibria calculations in the system K2O-FeO-MgO-Al2O3-SiO2-H2O-TiO2-Fe2O3. J. Metamorph. Geol. 18, 497–511.
White, R.W., Powell, R., Johnson, T.E., 2014b. The effect of Mn on mineral stability in metapelites revisited: new a–x relations for manganese-bearing minerals. J. Metamorph. Geol. 32, 809–828.
Yakymchuk, C., Brown, M., 2014. Consequences of open-system melting in tectonics. J. Geol. Soc. 171, 21–40.
Yakymchuk, C., Brown, M., Ivanic, T.J., Korhonen, F.J., 2013. Leucosome distribution in migmatitic paragneisses and orthogneisses: a record of self-organized melt migration and entrapment in a heterogeneous partially-molten crust. Tectonophysics 603, 136–154.